REVIEWS OF TOPICAL PROBLEMS

PACS number: 05.45.–a

Poincaré recurrence theory and its applications to nonlinear physics

V S Anishchenko, S V Astakhov

DOI: 10.3367/UFNe.0183.201310a.1009

Contents

Abstract. **Theoretical results concerning the Poincaré recurrence problem and their application to problems in nonlinear physics are reviewed. The effects of noise, nonhyperbolicity, and the size of the recurrence region on the characteristics of the recurrence time sequence are examined. Relations of the recurrence time sequence dimension to the Lyapunov exponents and the Kolmogorov entropy are demonstrated. Methods for calculating the local and global attractor dimensions and the Afraimovich–Pesin dimension are presented. Methods using the Poincaré recurrence times to diagnose the stochastic resonance and the synchronization of chaos are described.**

1. Introduction

The so-called Poincaré recurrence is one of the fundamental features pertaining to the time evolution of dynamical systems. Recurrence, according to Poincaré, implies that practically any phase trajectory leaving a point $\mathbf{x}_0$ of the phase space will pass infinitely many times arbitrarily close to its initial state as it evolves in time. Poincaré termed this type of motion in dynamical systems stable in the Poisson sense [1, 2].

Since the appearance of the pioneering papers by Poincaré, the analysis of statistical characteristics of the recurrence times has remained in the focus of modern science. The fundamental importance of this problem also follows from the fact that the idea that the system returns to the vicinity of its initial state as time progresses actually extends beyond its rigorous theoretical framework; in a certain sense, this idea has become one of the philosophical concepts of modern natural science.

A fundamental mathematical theory of the Poincaré recurrence has been developed. It describes statistics of the time of return both to the vicinity of the initial state [3] (the so-called local approach) and to a chosen set in the system phase space [4] (the global approach). A number of theorems generalizing and extending the classic Poincaré results [1, 2] are proved in [5–7]. In [8–10], it is proved theoretically that the probability density for the random sequence of recurrence times in the vicinity of the initial state obeys an exponential law. An important result concerning the connection between the mean recurrence time and the probability that the trajectory will stay in an ε-vicinity of a given initial state (the Kac theorem, local approach) is proved in [11, 12]. A number of important results obtained in studies of the recurrence time statistics in a stochastic layer in the vicinity of nonlinear resonances of Hamiltonian systems is proposed in the well-known paper [13]. Chetaev generalized the Poincaré result [1, 2] in Refs [14, 15] to the case where the right-hand sides of ordinary differential equations of the dynamical system are "in fact periodic with respect to time t with the same period" [15].

Relatively recently, studies considering a novel, so-called global, approach to the Poincaré recurrence problem have appeared [4, 16–18]. In the global approach, the Poincaré recurrence time averaged over all elements of a covering of the set as a whole is analyzed. The mean recurrence time in this case depends on the ensemble of initial points specified in each element of the covering and is a function of the entire set. Among the main characteristics of the Poincaré recurrence in the global approach is the fractal dimension of the set of

V S Anishchenko, S V Astakhov Physics Faculty,
Chernyshevsky Saratov State University,
ul. Astrakhanskaya 83, 410012 Saratov, Russian Federation
Tel. +7 (845-2) 210 720. Fax +7 (845-2) 210 721
E-mail: wadim@info.sgu.ru, astakhovsv@info.sgu.ru

Received 30 October 2012, revised 15 March 2013
Uspekhi Fizicheskikh Nauk **183** (10) 1009 – 1028 (2013)
DOI: 10.3367/UFNr.0183.201310a.1009
Translated by S D Danilov; edited by A M Semikhatov

recurrence times, called the Afraimovich–Pesin (AP) dimension in Refs [19, 20].

We note that a direction of research based on the method of recurrence plots, which in essence relies on the Poincaré recurrence concept, has been successfully developing recently [21, 22].

The references mentioned above mainly represent rigorous mathematical results, which lay the basis for much experimental work on numerical modeling of the Poincaré recurrence statistics for concrete systems. We are interested in work on the analysis of Poincaré recurrence statistics in low-dimensional discrete dissipative systems with a chaotic attractor (see, e.g., Refs [23–26]). Chaotic systems are characterized by Poisson stability and are ergodic because of the presence of mixing. This allows using mathematical results to analyze the results of computational experiments. However, the systems being studied do not, as a rule, fully satisfy the properties of hyperbolicity, can be irreversible, and can involve complications related to the existence of a probability measure; therefore, the experimental research on such systems would also enable estimates of the extent to which the rigorous results are applicable to them.

This review presents numerical modeling results concerning statistical characteristics of the Poincaré recurrence in discrete maps based on both local and global approaches. It offers an analysis of the impact of an external noise source on the characteristics of the recurrence times, including the AP dimension, and it corroborates the correspondence between the AP dimension and the positive Lyapunov exponents (in the absence of noise) and the relative Kolmogorov entropy (for systems with noise). We discuss applied aspects of the Poincaré recurrence theory for carrying out the tasks of diagnosing stochastic resonances, synchronization, and computing the dimensions of chaotic attractors.

2. Main theoretical results concerning the Poincaré recurrence

The problem of Poincaré recurrence, as discussed in the Introduction, has been fully solved and described in the mathematical literature for ergodic systems with a given probability measure. The fundamental mathematical result is expressed by the Kac theorem [11, 12], which states that the mean time $\langle \tau_{\mathrm{r}}(\varDelta) \rangle$ for returning to some subdomain $\varDelta$ belonging to the phase space domain under consideration is inversely proportional to the probability of the phase trajectory visiting this domain $P(\varDelta)$:

$$\big\langle \tau_{\mathrm{r}}(\varDelta) \big\rangle = \frac{1}{P(\varDelta)} \,. \tag{1}$$

The proof of statement (1) was given under the conditions that the system has an ergodic probability measure and is reversible. No constraint was imposed on the domain of returns $\varDelta$. Further research has indicated that the condition that the system is reversible is not a necessary one. A proof of Kac theorem (1) proposed in [4] does not rely on the reversibility, exploiting the ergodicity only.

We here analyze the recurrence for the domain $\varDelta$ defined as an N-dimensional cube (N is the dimension of the system phase space) with an edge ε, centered around the initial state $\mathbf{x}_0$. As is discussed in what follows, for a small $\varepsilon \ll 1$, the probability that the trajectory enters the ε-vicinity of the initial state can be expressed as

$$P(\varepsilon) \simeq p(\mathbf{x}_0)\varepsilon^{d_{\mathrm{f}}} \,, \tag{2}$$

where $p(\mathbf{x}_0)$ is the probability density function and d_{f} is the fractal dimension of the set of possible states. Then, defining the region $\varDelta$ as a cube with the edge ε and taking $P(\varepsilon)$ in form (2), we arrive at an alternative form of the Kac theorem:

$$\big\langle \tau_{\mathrm{r}}(\mathbf{x}_0, \varepsilon) \big\rangle \simeq \frac{1}{p(\mathbf{x}_0)}\, \varepsilon^{-d_{\mathrm{f}}} \,, \quad \varepsilon \ll 1 \,. \tag{3}$$

Equation (3) plotted in the double logarithmic scale describes a straight line with the slope $k = -d_{\mathrm{f}}$, which is used in carrying out numerical experiments and analyzing their results. The averaging is performed in Eqn (1) over an ensemble, or over time for ergodic systems. For dynamical systems, the sequence of first recurrence times has the form $\tau_{\mathrm{r}k} = t_{k+1} - t_k$ $(k = 1, 2, \ldots, k_{\max})$ and the mean time is

$$\big\langle \tau_{\mathrm{r}}(\varepsilon) \big\rangle = \frac{1}{k_{\max}} \sum_{k=1}^{k_{\max}} (t_{k+1} - t_k) \,, \quad k_{\max} \gg 1 \,, \tag{4}$$

where the index k corresponds to the discrete time of the trajectory visiting the ε-vicinity.

An important mathematical result is the proof of the statement that the probability density for the random process of returns obeys the exponential law [8–10]

$$p(\tau_{\mathrm{r}}) = \frac{1}{\langle \tau_{\mathrm{r}} \rangle} \exp\left(-\frac{\tau_{\mathrm{r}}}{\langle \tau_{\mathrm{r}} \rangle} \right), \quad \tau_{\mathrm{r}} \geqslant \tau_{\mathrm{r}}^* \,, \tag{5}$$

for ergodic systems that have the mixing property, where τ_{r}^* is a certain value of τ_{r}. Law (5) describing the probability distribution of a random sequence of returns to the ε-vicinity of some given point holds in the limit $\varepsilon \to 0$ for all $\tau_{\mathrm{r}} \geqslant \tau_{\mathrm{r}}^*$.

We note that to prove Kac theorem (1), it suffices to assume that a probability measure exists, but the proof of Eqn (5) relies on a stronger assumption, the existence of mixing. Mixing implies ergodicity, but the converse is not true. For example, motion on a two-dimensional torus is ergodic if the rotation number is irrational, but mixing is absent. In this review, we analyze chaotic systems that have mixing by definition and are therefore ergodic.

The discussion above pertains to the problem of returns to a given ε-vicinity of a selected point of the set explored and, consequently, to the description of local Poincaré returns. There is an alternative approach to the Poincaré recurrence problem, based on the subdivision of the entire set into ε-elements and subsequent averaging of minimum return times over the subdivisions. Because averaging involves the entire set, the approach can be termed global. The mathematical theory of the global approach was proposed in Refs [4, 16–18].

The essence of the global approach is as follows. The selected set of phase trajectories of a dynamical system (for example, its attractor) is covered by cubes (or spheres) $\varepsilon \ll 1$ in size. The covering must be complete for the set studied. For each element of the covering ε_i $(i = 1, 2, \ldots, m)$, the minimum time of the first recurrence of the phase trajectory in the ε_i-vicinity, $\tau_{\inf}(\varepsilon_i)$, is determined. Then the mean first recurrence time over the entire set of covering elements ε_i is found:

$$\big\langle \tau_{\inf}(\varepsilon) \big\rangle = \frac{1}{m} \sum_{i=1}^{m} \tau_{\inf}(\varepsilon_i) \,. \tag{6}$$

It follows that [16]

$$\langle \tau_{\rm inf}(\varepsilon) \rangle \sim \phi^{-1}(\varepsilon^{d/\alpha_c}), \tag{7}$$

where α_c is the dimension of recurrence times introduced by Afraimovich and Pesin [16–18] and d is the dimension of the set considered. The function ϕ in Eqn (7) can take one of the forms

$$\phi(t) \sim \frac{1}{t}, \quad \phi(t) \sim \exp(-t), \quad \phi(t) \sim \exp(-t^2), \quad \ldots, \tag{8}$$

depending on the topological entropy h_t of the system [27] and on the multifractality of the set studied, whenever it is relevant. If the topological entropy $h_t = 0$, then $\phi(t) \sim 1/t$ and it follows from Eqn (7) that

$$\langle \tau_{\rm inf}(\varepsilon) \rangle \sim \varepsilon^{-d/\alpha_c}. \tag{9}$$

If $h_t > 0$, then $\phi(t)$ is commonly written as an exponential, $\phi(t) \sim \exp(-t)$. Equation (7) can then be written in the form [28]

$$\langle \tau_{\rm inf}(\varepsilon) \rangle \sim -\frac{d}{\alpha_c} \ln \varepsilon. \tag{10}$$

As is well known [29], the topological entropy h_t is the upper bound for the Kolmogorov–Sinai (KS) entropy, which is in turn defined by the positive Lyapunov exponents λ^+. Hence, it follows that for chaotic dynamical systems with exponentially divergent trajectories, the topological entropy is positive ($h_t > 0$) and Eqn (10) is valid. For chaotic systems, expression (9) is valid only for critical values of the parameter for which the KS entropy (and hence h_t) vanishes.

Such are, in brief, the main results related to the Poincaré recurrence problem used in this review. In the literature on nonlinear dynamics, in addition to theoretical results, numerous issues of practical relevance are discussed. Among them, we mention the use of recurrence times to solve the problem of controlling chaos (the so-called targeting problem [26]) and the use of the AP dimension to diagnose synchronism between coupled chaotic oscillators [28, 30] and to diagnose the effect of stochastic resonance for noise-induced transitions in bistable systems [31]. Because rigorous results have been obtained only for hyperbolic systems with a given probability measure, the analysis of Poincaré returns in quasi-hyperbolic systems is important.

We mention an important detail. Numerical modeling of the Poincaré recurrence relies on algorithms and programs that do not require immediate knowledge of the probability measure. For this reason, in numerical solutions, the results are usually not compared with the form and evolution of the probability measure when the system parameters are varied and external noise is added. This juxtaposition is undoubtedly necessary because, as follows from the mathematical theory, just the changes in the probability density $p(x)$ must determine the results.

3. Local approach. Kac theorem in the presence of external noise

As a system for study, we consider a cubic map with a chaotic quasi-attractor [32]

$$x_{n+1} = (\alpha x_n - x_n^3) \exp\left(-\frac{x_n^2}{B}\right) + \sqrt{2D}\,\xi_n, \tag{11}$$

where α is a control parameter, $B = 10$ is the coefficient in the exponent introduced to limit the growth rate of x_n, D is the noise intensity, and ξ_n is the source of bounded white noise.

Map (11), which is one of the basic models of bistable systems demonstrating the effect of stochastic resonance [33], allows constructing the probability density $p(x)$ numerically and carrying out a detailed comparison between the characteristics of Poincaré recurrences and theoretical predictions. Importantly, map (11), being a system with a quasi-attractor [32], does not belong to the class of hyperbolic systems [34]. Therefore, the analysis of recurrences in system (11) enable us to learn whether the results of the theory developed for hyperbolic systems are applicable to nonhyperbolic ones.

Bistability in system (11) allows modeling the crisis of two symmetric attractors that occurs when the parameter α passes through a certain critical value α^* [32, 35]. The crisis can be induced by noise of a certain intensity D for $\alpha < \alpha^*$. In view of the importance of this effect for studies of stochastic resonance, we analyze the characteristics of Poincaré recurrences in the regime of the noise-induced crisis of attractors [35].

As can be seen from Fig. 1, which illustrates the evolution of the probability density $p(x, D)$ in system (11) for $\alpha = 2.7$, two symmetric attractors ($x_n \to -x_n$) are realized in this system for $D < 10^{-4}$. At $D = 1.1 \times 10^{-4}$, the attractors merge into one. From the figure, it is apparent that as the intensity D increases, the function $p(x_n)$ changes noticeably. This must result in corresponding changes in qualitative characteristics of the recurrence times. We note that in numerical experiments, the density $p(x_n)$ was determined approximately,

$$p(x_n) \approx \frac{\Delta P(x_n \pm \Delta x_n/2)}{\Delta x_n}, \tag{12}$$

where ΔP is the probability of the trajectory visiting the vicinity of the point x_n and $\Delta x_n \leqslant 10^{-3}$ is the size of this vicinity. The computational results for $p(x_n)$ in the entire domain of x were normalized such that the sum of all probabilities is zero.

We select five points ($i = 1, \ldots, 5$) on the attractor of system (11) with different values of the probability density $p(x_0^i)$: $x_0^1 = 0.37$, $x_0^2 = 0.65$, $x_0^3 = 0.95$, $x_0^4 = 1.25$, and $x_0^5 = 1.46$. We compute the mean recurrence times $\langle \tau_r(\varepsilon) \rangle$ in the ε-vicinity of these points for $\varepsilon = 0.1$ as functions of the noise intensity D. From the computational results presented in Fig. 2, it follows that 1) on passing the threshold value as the noise increases, $D > 10^{-4}$, an abrupt increase in the mean recurrence time for all five points is observed; 2) the mean recurrence time behaves in a principally nonlinear way with an increase in the noise intensity: it may increase or decrease as a function of the noise intensity. From a comparison of Fig. 1 and Fig. 2, it can be clearly seen that an increase in $\langle \tau_r(D) \rangle$ is caused by a decrease in $P(x_n)$, while a decrease in $\langle \tau_r(D) \rangle$ is caused by an increase in $P(x_n)$, in perfect agreement with Eqn (1).

We now turn to the character of the dependence $\tau_r(\varepsilon)$ and compare the computational results with theoretical ones. With this aim, consider a fixed point $x_0^3 = 0.65$. We compute mean recurrence times for the ε-vicinity of x_0 for ε ranging from 10^{-2} to 10^{-1}. The results of numerical experiments are displayed in Fig. 3.

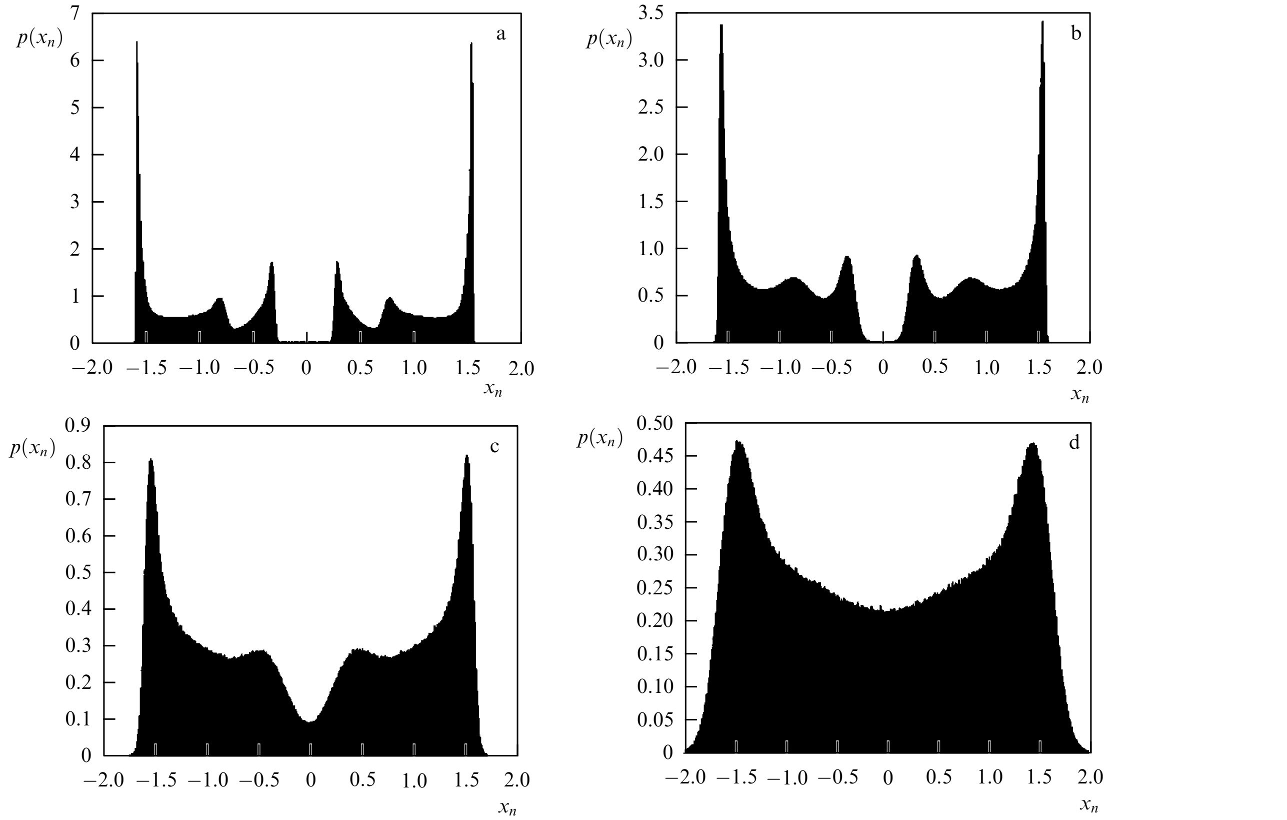

Figure 1. Probability density $p(x_n)$ of the attractors of system (11) for noise with the intensity (a) $D = 10^{-5}$, (b) $D = 10^{-4}$, (c) $D = 10^{-3}$, and (d) $D = 10^{-2}$. There are two symmetric attractors in panels a and b, and a merged attractor in panels c and d.

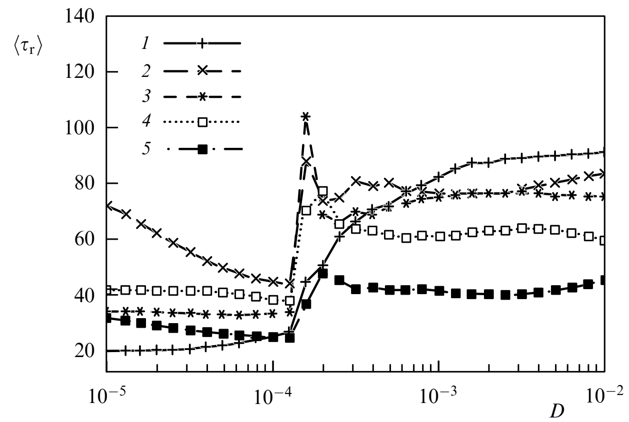

Figure 2. Comparison of the dependence of the mean recurrence times $\langle\tau_r\rangle$ on the noise intensity for five selected points on the attractor.

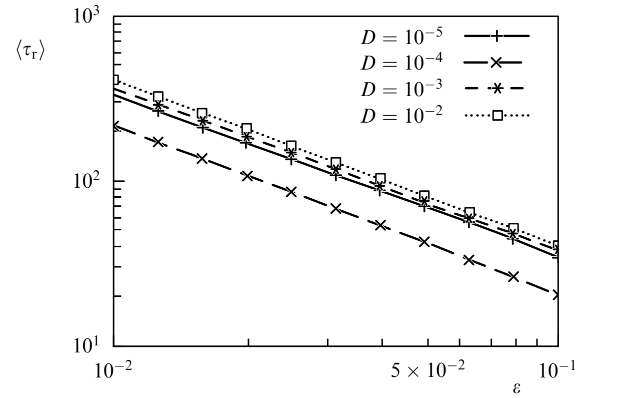

Figure 3. Dependence of the mean recurrence time $\langle\tau_r\rangle$ on ε for five points selected on the attractor (in logarithmic scales).

By performing a least-squares fit, we find that the dependences plotted in Fig. 3 in a double logarithmic scale correspond to the straight lines

$$\lg\langle\tau_r(\varepsilon)\rangle = \lg C(D) - k\lg\varepsilon\,, \tag{13}$$

with $k = 1.00 \pm 0.02$ for all lines in Fig. 3, and the noise has an impact only on the coefficients C:

$$\begin{aligned} &C_1 = 3.756\ (D = 10^{-5})\,, \quad C_2 = 1.958\ (D = 10^{-4})\,, \\ &C_3 = 3.900\ (D = 10^{-3})\,, \quad C_4 = 4.012\ (D = 10^{-2})\,. \end{aligned} \tag{14}$$

The coefficients $C(D)$ in (14) and the coefficient $k = 1.00 \pm 0.02$ are obtained by direct approximation of the data plotted in Fig. 3. If the Kac theorem also holds in the case where system (11) contains a source of noise, the coefficients $C(D)$ in (14) must correspond to the $p^{-1}(x_0)$ values given by the distributions plotted in Fig. 1 and computed for D in the range $10^{-5}-10^{-2}$. Computations indicate that the values of coefficients derived from the probability density $p(x_0, D)$ agree with approximation (14) within $\pm 5\%$.

In the case considered, expression (1) can be written as

$$\langle\tau_r(\varepsilon)\rangle = C\varepsilon^{-1}\,, \qquad C = \frac{1}{p(x_0, D)}\,. \tag{15}$$

We conclude that the experimental data in Fig. 3, which are approximated by Eqns (13) and (14), fully agree with (1) both

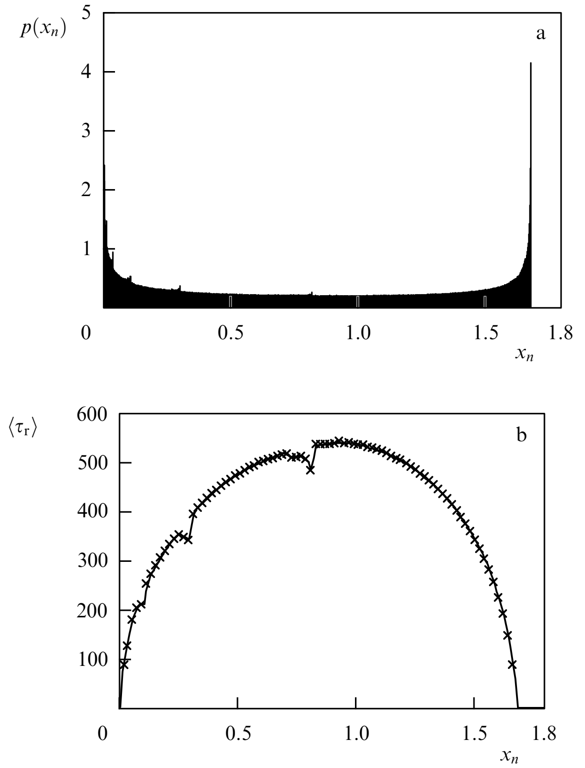

Figure 4. (a) Probability density $p(x_n)$ on the attractor of system (11) for $\alpha = 2.84$ and $D = 0$. (b) Mean recurrence time for the ε-vicinity of the point x_n for $\varepsilon = 0.01$.

in the absence and in the presence of additive noise in nonhyperbolic system (11).

A distinctive feature of the local approach is that the recurrence times depend on the vicinity of the selected point on the attractor $\langle\tau(x_0)\rangle$. This fact is very important for certain applied problems, such as chaos control (see, e.g., [26]). For example, Fig. 4 depicts computational results for $\langle\tau_r\rangle$ as a function of a point x on the attractor of system (11). We select the regime of merged attractors ($\alpha = 2.84$) in the absence of noise. The recurrence time $\langle\tau_r\rangle$ for $0 \leqslant x_n \leqslant 1.7$ (Fig. 4b) fully corresponds to changes in $p(x_n)$ (Fig. 4a) and can be computed based on the Kac theorem. On adding noise, the correspondence to the Kac theorem is preserved.

This result, generally speaking, could be anticipated. If we regard system (11) with noise as being represented by a stationary random process, then we are dealing with the equivalent of an ergodic system, and in this case the Kac theorem holds. Hence, the results described above provide an experimental proof that the fundamental Kac theorem remains valid for noisy systems.

4. Probability density of recurrence times. Impact of noise

As discussed in Section 2, for a given chaotic attractor domain, the times of the first Poincaré recurrence τ_r $\Delta = x_0 \pm \varepsilon/2$ satisfy exponential law (5) in the limit $\varepsilon \to 0$ for $\tau_r \geqslant \tau_r^*$, where τ_r^* is some value of the recurrence time [8–10, 25, 36]. We write (5) in the form

$$p(\tau_r) = C\exp(-\gamma\tau_r)\,. \tag{16}$$

We test the correspondence between Eqn (16) and law (5) in a numerical experiment in terms of the coefficients C and γ

Table 1. Comparison of the computed $P(\Delta_i)$ with the data of approximation (17) for the points x_0^i selected on the attractor ($\delta_{P,\gamma} = |P(\Delta_i) - \gamma_i|/P(\Delta_i)$, $\delta_{\gamma,C} = |\gamma_i - C_i|/\gamma_i$).

i	x_0^i	$P(\Delta_i)$	γ_i	C_i	$\delta_{P,\gamma}$, %	$\delta_{\gamma,C}$, %
1	0.37	7.468×10^{-3}	6.872×10^{-3}	6.26×10^{-3}	7.9	8.9
2	0.65	3.071×10^{-3}	3.174×10^{-3}	3.24×10^{-3}	3.3	2.0
3	0.95	5.224×10^{-3}	5.532×10^{-3}	5.87×10^{-3}	5.8	6.1
4	1.25	4.091×10^{-3}	4.241×10^{-3}	4.40×10^{-3}	3.6	3.7
5	1.46	9.714×10^{-3}	8.361×10^{-3}	7.13×10^{-3}	13.9	14.7

in the cases with and without the external noise [37]. In the absence of noise, the coefficients C and γ depend on the choice of x_0 and ε. In the limit $\varepsilon \to 0$, $P(\varepsilon)$ also tends to zero and the equality $\gamma = P(\varepsilon) = 1/\langle\tau_r\rangle$ holds, where $\langle\tau_r\rangle$ is the recurrence time mean value [25, 36]. In numerical experiments for small but finite $\varepsilon \ll 1$, this equality can be violated, depending on the precise values of ε and the system being studied. The coefficient γ can be determined experimentally by considering Eqn (16) in the logarithmic scale. The slope of the linear dependence

$$\ln p(\tau_r) = \ln C - \gamma\tau_r \tag{17}$$

yields the value of γ, while its intercept gives C.

We consider the results for $p(\tau_r)$ computed for map (11). We select the same five points x_0^i as in Section 3, on the attractor of system (11), and compute the respective probability densities $p_i(\tau_r)$ for their vicinities $\Delta_i = x_0^i \pm \varepsilon/2$, setting $\varepsilon = 10^{-2}$. We begin with the case of no noise ($D = 0$) taking the parameter value $\alpha = 2.7$ (before the crisis of attractors). The results are plotted in Fig. 5a. For $\tau > 25$, all the dependences can be approximated by straight lines, yielding the slopes γ_i and the coefficients C_i. The computations show that the coefficients γ_i agree rather well with the probabilities $P(\Delta_i)$ for $\varepsilon = 10^{-2}$. The comparison is presented in Table 1, where the two last columns give the values of the quantities $|P(\Delta_i) - \gamma_i|/P(\Delta_i)$ and $|\gamma_i - C_i|/\gamma_i$ characterizing errors.

As follows from Table 1, the computed probabilities $P(\Delta_i)$ and the coefficients γ_i and C_i obtained by approximating the results presented in Fig. 5a are approximately equal to each other (with an error of less than 15%). Special computations have shown that this error decreases as ε decreases. It can be assumed that in the limit $\varepsilon \to 0$, the equality $\gamma = C = P(\Delta)$ is satisfied. In that case, expression (16) can be rewritten in the form

$$p(\tau_r) = \gamma\exp(-\gamma\tau_r) = \frac{1}{\langle\tau_r\rangle}\exp\left(-\frac{\tau_r}{\langle\tau_r\rangle}\right), \tag{18}$$

which just coincides with law (5).

We consider the influence of noise on the distribution of recurrence times $p(\tau_r)$. As follows from Fig. 5b, the density $p(\tau_r)$ for $\tau_r \geqslant 20$ qualitatively repeats the dependences in the absence of noise plotted in Fig. 5a. The difference between the results lies in the change in the slope (coefficients γ_i) in the presence of noise. This allows concluding that in the presence of noise, the exponential law in (5), (16)–(18) remains valid. It is only necessary to keep in mind that the coefficient γ depends on the noise intensity D and the size ε of the interval around the given point x_0^i ($\gamma = \gamma(D, x_0^i, \varepsilon)$).

Detailed computations performed for system (11) for $\alpha = 2.7$ and the noise level $D = 10^{-5} - 10^{-4}$ (before the crisis of attractors) have shown that $p(\tau_r)$ obeys law (5). The

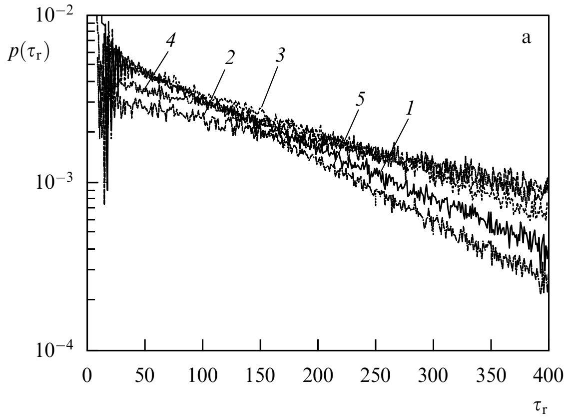

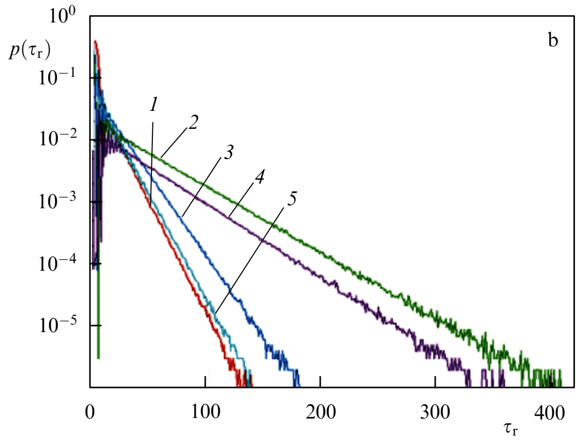

Figure 5. Probability density for the recurrence times at five points on the attractor computed for $\alpha = 2.7$, $D = 0$, and $\varepsilon = 10^{-2}$ in system (11) (a) in the absence of noise ($D = 0$) and (b) in the presence of noise with the intensity $D = 10^{-5}$.

coefficients γ and C in (16) are close to the values of the probability $P(\varepsilon)$ in the presence of noise. For example, the error is less than 5% for $\varepsilon = 10^{-5}$. The impact of noise modifies the probability measure, and $P(\varepsilon)$ varies, in contrast to $P(\varepsilon)$ in the unperturbed system.

As the intensity of noise increases past the value $D = 1.1 \times 10^{-4}$ at which the attractors merge, the results undergo qualitative changes. The crisis of attractors shifts the dynamics of map (11) to the regime of chaos–chaos intermittance. The trajectory $\{x_n\}$ of the system spends some time in the domain of one of the two symmetric attractors, randomly hopping between them under the action of noise [32]. The system acquires two characteristic time scales, a global and a local one. Their presence explains the character of the dependences $P(\tau_r)$ (Fig. 6), which clearly manifest the regions of local ($\tau_r < 100$) and global ($\tau_r < 100$) dynamics.[1] Each of these dependences can be approximated by two straight lines, which give the respective coefficients $\gamma_i^{1,2}(x_0^i)$. Computations show that for $\varepsilon = 0.1$ in the neighborhood of all five points x_0^i, the inequalities

$$\gamma^1 > P(\varepsilon) > \gamma^2 \tag{19}$$

hold. For example, for $x_0^4 = 1.25$ and $\varepsilon = 0.1$, we have $\gamma^1 = 0.457$, $\gamma^2 = 0.004$, and $P(\varepsilon) = 0.035$. The departure of the dependences $p(\tau_r)$ in Fig. 6 from behavior (18) stems from the finiteness of the quantity $\varepsilon = 10^{-1}$ [37].

[1] We mention the results in Ref. [13], where a qualitatively similar effect was discovered by analyzing recurrences in a stochastic layer in the vicinity of a nonlinear resonance.

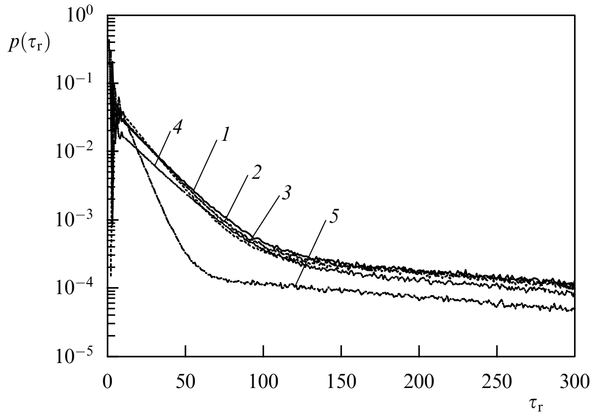

Figure 6. Distributions $p(\tau_r)$ for $D = 10^{-3}$ (after the crisis of attractors) computed for $\alpha = 2.7$ and $\varepsilon = 0.1$ for the five selected points.

We turn now to Fig. 7, which plots the results of computations of $p(\tau_r)$ for the point $x_0^4 = 1.25$ ($i = 4$) and various values of ε. As can be seen, with a reduction in ε, the influence of intermittency noticeably decreases, practically disappearing for $\varepsilon = 10^{-3}$. In this case, γ^1 and γ^2 also decrease, tending to the value $P(\varepsilon)$. For example, for $\varepsilon = 10^{-3}$, we obtain $\gamma^1 = 0.0043$, $\gamma^2 = 0.00033$, and $P(\varepsilon) = 0.00035$. We therefore believe that in the limit $\varepsilon \to 0$, the equality $\gamma^1 = \gamma^2 = P(\varepsilon)$ is practically satisfied. However, we note that in this case $P(\varepsilon) \to 0$, and the recurrence times sharply increase, tending to infinity. It can be assumed that exponential law (5) holds in the limit $\varepsilon \to 0$ for purely dynamical systems as well as for systems affected by noise.

The results presented above lead to an important conclusion. For small but finite values of ε, deviations of $p(\tau_r)$ from distribution law (5) can occur depending on particular physical characteristics of the system, which may be used for solving applied tasks.

5. Diagnostics of the effect of stochastic resonance using the Poincaré recurrence time distribution

As demonstrated in Section 4, the recurrence time probability density obeys exponential law (5) for infinitely small $\varepsilon \to 0$. For small but finite ε, this law can be violated, as is suggested to by the results presented in Fig. 7 and by the data in Refs [24, 35, 37]. The probability density $p(\tau_r)$ computed for a finite ε may reflect certain important features of the system dynamics. For example, the dependence $p(\tau_r)$ for $\varepsilon = 10^{-1}$ (Fig. 7a) clearly reflects the intermittent character of dynamics in system (11) realized after the crisis of attractors. We demonstrate that just these properties of $p(\tau_r)$ can be used for $0 < \varepsilon < 1$ to diagnose the regime of stochastic resonance (SR).

The classical phenomenon of SR is described in Refs [33, 38] using the example of an overdamped bistable Kramers oscillator

$$\dot{x} = x - x^3 + A\cos(\Omega t) + \sqrt{2D}\,\xi(t)\,, \tag{20}$$

where A and Ω are the amplitude and frequency of weak external forcing and D is the intensity of a δ-correlated noise $\xi(t)$.

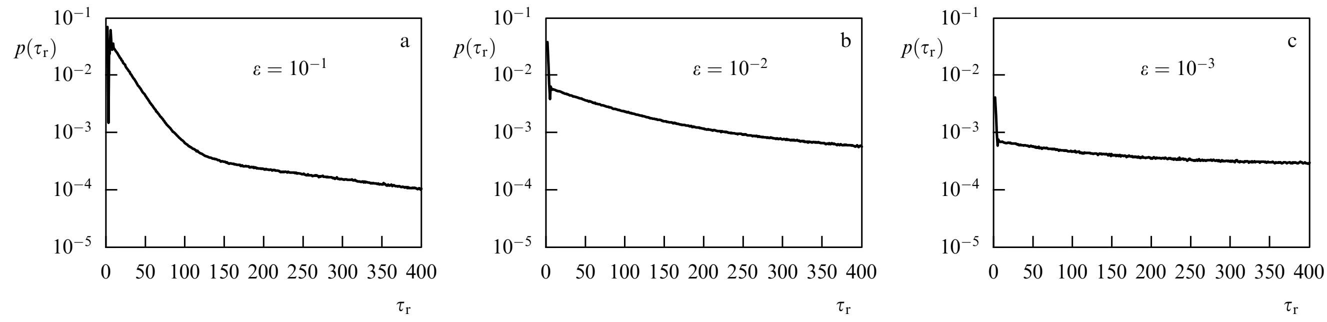

Figure 7. Evolution of the probability density $p(\tau_r)$ as the neighborhood size ε decreases for the attractor point $x_0^4 = 1.25$ for $\alpha = 2.7$ and $D = 10^{-3}$.

It was established and then repeatedly confirmed experimentally (see Ref. [39] and the references therein) that in the regime of noise-induced transitions, the intensity of the periodic component in the spectrum of the output signal $x(t)$ attains a maximum at a certain optimal noise level $D = D^*$. It was shown that the optimal noise level D^* in the SR regime is associated with the Kramers transition frequency [40], which is close to the external signal frequency Ω in Eqn (20). The dependence of the signal-to-noise ratio (SNR) on the noise intensity D has a shape resembling the resonance curve with a maximum at $D = D^*$, which was the reason why the name stochastic resonance was chosen.

Discrete system (11) considered in this review is one of the simplest systems in which the SR effect occurs both because of noise-induced transitions in the classical case and because of variations in the control parameter in the absence of noise (under the conditions of the attractor crisis) [32, 39, 41]. To realize the SR effect, we augment system (11) with an additive periodic forcing:

$$x_{n+1} = (ax_n - x_n^3) \exp\left(-\frac{x_n^2}{b}\right) + A \sin(\Omega n) + \sqrt{2D}\,\xi_n\,. \quad (21)$$

System (21) represents a one-dimensional cubic map excited by a small ($A \ll 1$) periodic signal and a source ξ_n of δ-correlated noise of the intensity D. The exponential factor in Eqn (21) is introduced, as previously in Eqn (11), to avoid the drift of trajectories toward large values of x_n.

We consider the dynamics of system (21) in the absence of perturbations ($A = D = 0$). If $a < a^* = 2.839$, two chaotic attractors, symmetric with respect to the saddle equilibrium point $x_n^0 = 0$, coexist in the system. At $a = a^*$, bifurcation occurs, the attractors merge, and intermittent chaos–chaos behavior emerges. Stationary probability densities $p(x)$ before and after the merging are plotted in Figs 8a and 8b.

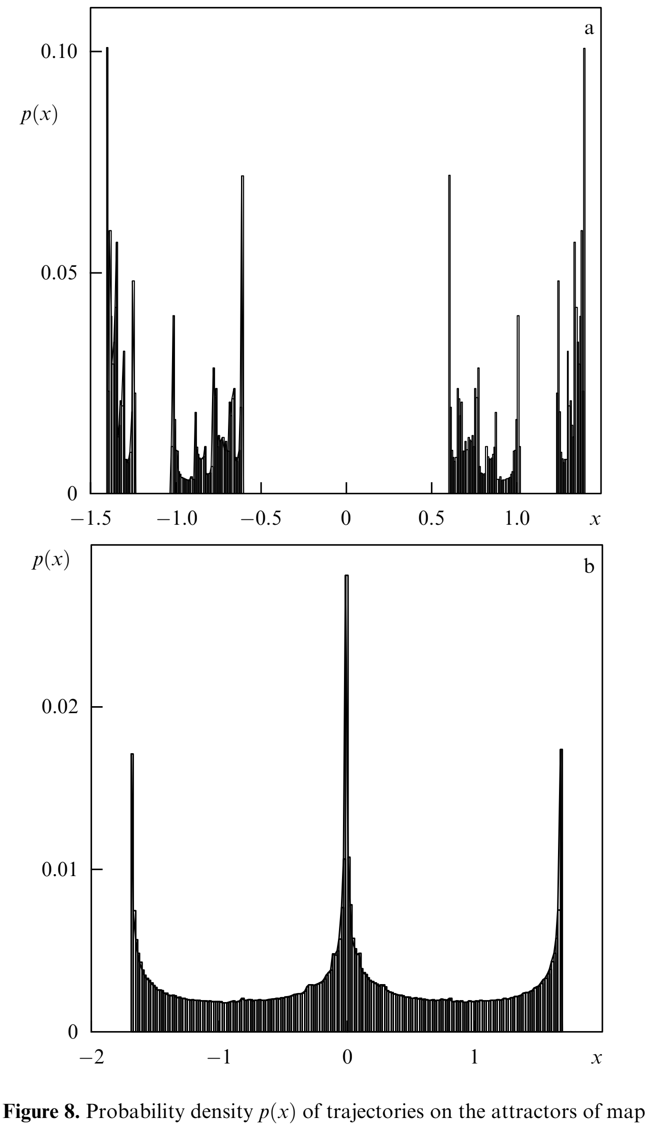

Figure 8. Probability density $p(x)$ of trajectories on the attractors of map (21) with $A = D = 0$, $b = 10$ for parameter values (a) $a = 2.5$ and (b) $a = 2.84$.

The effect of stochastic resonance in system (21) is thoroughly described and explored in Refs [38, 39, 41]. We mention that the effect has been diagnosed by the classical filtration method (the method of two states) with the help of a telegraph signal model. As can be seen from Fig. 9a, the SR effect induced by noise (curve *1*) attains a maximum at the optimal noise intensity $D^* \approx 0.01$. Without noise, the SR effect is observed (Fig. 9b) for the control parameter $a \approx 2.84$ (curve *1*) [41].

We discuss another possibility of diagnosing SR by using a computed probability distribution for the Poincaré recurrence times [31]. We perform computations of $p(\tau_r)$ for some region $x_0 \pm \varepsilon/2$, taking $x_0 = -1.1$ and varying ε.

Figure 10a plots the density $p(\tau_r)$ found numerically for $\varepsilon = 10^{-1}$ (curve *1*) and $\varepsilon = 10^{-4}$ (curve *2*). The finiteness of ε has the effect that the distributions $p(\tau_r)$ are different from exponential law (5), which is especially clearly illustrated by curve *1* in Fig. 10a. One of the differences lies in the fact that the plot of $p(\tau_r)$ contains two distinct time intervals ($\tau_r \leqslant 160$ and $\tau_r > 160$) within which the decay rates for $p(\tau_r)$ (as

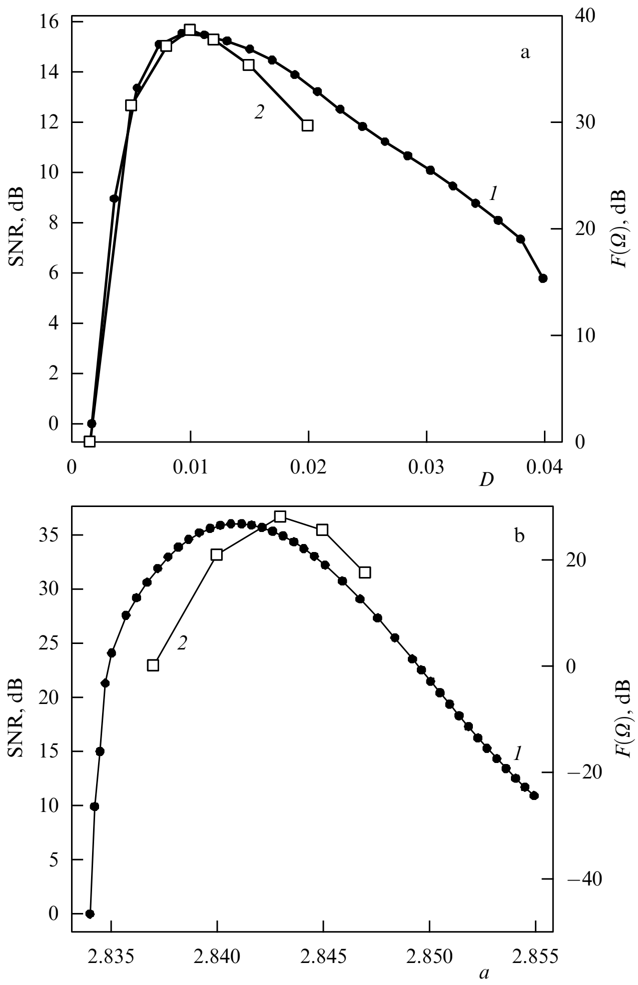

Figure 9. The SNR (curves *1*) and the behavior of the maximum $F_{\rm m}(\omega) = F(\Omega)$ of the spectral function $F(\omega)$ (curves *2*) as a function of (a) the noise intensity D for $a = 2.5$, $A = 0.05$, and $\Omega = 0.1$ and (b) the control parameter a for $D = 0$, $A = 0.005$, and $\Omega = 0.1$ [41].

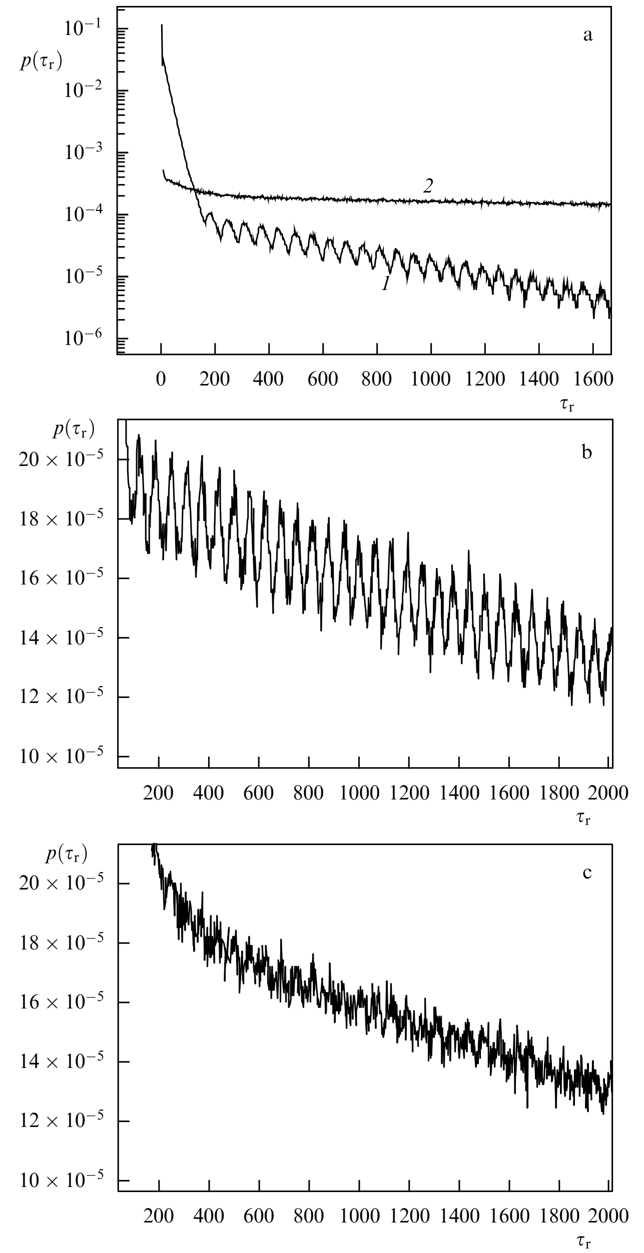

Figure 10. The probability density for the Poincaré recurrence $p(\tau_{\rm r})$: (a) for $\varepsilon = 10^{-1}$ (curve *1*) and $\varepsilon = 10^{-4}$ (curve *2*) for $a = 2.837$, (b) in the resonance case $a = 2.843$, and (c) in the off-resonance case $a = 2.837$. In panels a and b, $\Omega = 0.1$, $b = 10$, $A = 0.005$, $D = 0$, and $\varepsilon = 10^{-4}$.

discussed above) are essentially different. Another distinction is the presence of a periodic modulation of the function $p(\tau_{\rm r})$ in the region $\tau_{\rm r} > 160$ with the period $T \approx 2\pi/\Omega = 62.8$. As noted above, for finite values of ε, the distribution $p(\tau_{\rm r})$ carries information on the properties of the dynamics of the system being explored. In our case, the appearance of two time intervals with different slopes of $p(\tau_{\rm r})$ is a reflection of intermittency in the system [35, 37]. The presence of a periodic modulation is due to the nonautonomous character of system (21). It can be assumed that in the limit $\varepsilon \to 0$, the distribution law for $p(\tau_{\rm r})$ is exponential on average. To a certain degree, this is corroborated by curve *2* in Fig. 10a, computed for $\varepsilon = 10^{-4}$. It is noteworthy that the periodic modulation of the function $p(\tau_{\rm r})$ is also preserved in this case, although the modulation amplitude decreases substantially.

We use the fact that the function $p(\tau_{\rm r})$ is modulated at a frequency close to the frequency Ω of the external signal in Eqn (21). Hence, the Fourier spectrum of $p(\tau_{\rm r})$,

$$F(\omega) = \frac{1}{2\pi}\int_0^{\infty} p(\tau_{\rm r}) \exp(-{\rm i}\omega\tau_{\rm r})\,{\rm d}\tau_{\rm r}\,, \tag{22}$$

should exhibit a peak at the frequency $\omega = \Omega$. Computations have corroborated this fact. It is natural to suppose that the peak amplitude attains a maximum in the SR regime, which has also been confirmed by computations [31].

To compute the spectrum $F(\omega)$ of $p(\tau_{\rm r})$ we selected values $10^{-4} \leqslant \varepsilon \leqslant 10^{-3}$. In this case, the distribution $p(\tau_{\rm r})$ turns out to be defined on a rather long time interval, $0 < \tau_{\rm r} \leqslant 80{,}000$, which allows computing $F(\omega)$ more reliably. As an illustration, we present the data that correspond to the SR regime in system (21) in the absence of noise ($a = 2.843$, $D = 0$). Figure 10b shows a magnified part of Fig. 10a. The spectrum $F(\omega)$ computed in this case is presented in Fig. 11a. There is a well-expressed peak at the frequency Ω in the spectrum $F(\omega)$, which corresponds to a practically periodic modulation in $p(\tau_{\rm r})$. If we depart from the optimal regime by shifting the parameter a to $a = 2.837$, the following picture is observed: the probability distribution $p(\tau_{\rm r})$ is modulated in a more intricate way (see Fig. 10c) and,

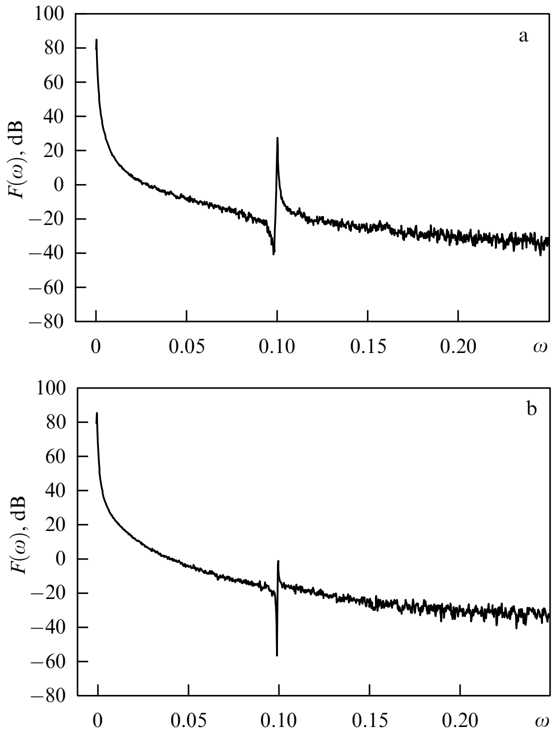

Figure 11. Amplitude spectra of the function $p(\tau_r)$ for the distributions of $p(\tau_r)$ corresponding to Fig. 10b for (a) $a = 2.843$ and (b) $a = 2.837$. The parameters are $b = 10$, $A = 0.005$, $\Omega = 0.1$, $D = 0$, and $\varepsilon = 10^{-3}$.

as a consequence, the peak at the frequency Ω in the spectrum $F(\omega)$ decreases substantially in amplitude (Fig. 11b). Thus, if we carry out the computations described above for system (21), we can diagnose the effect of SR and compare the results with those obtained previously.

The results of computations of the spectral amplitude $F(\Omega)$ in the case of a noise-induced SR (curve *2* in Fig. 9a) and when the parameter a is varied in the absence of noise (curve *2* in Fig. 9b) qualitatively agree with the results of computations in Refs [32, 39, 41].

The result obtained here can easily be understood from the experimental standpoint, as well as from the standpoint of the SR effect theory and could possibly be predicted. The SR effect can hopefully be proved by resorting, for example, to the results in Ref. [42]. But the results described above do not rely on the global analysis of the effect of switching in the SR regime, which underlies the theory, but are obtained based on the local approach; in this sense, they are interesting from the standpoint of revealing peculiarities of Poincaré returns to a finite domain.

Relatedly, the SR effect can be diagnosed in a numerical experiment by computing the spectral function $F(\omega)$ of the probability density for the Poincaré recurrence times in a finite ε-vicinity of an arbitrary point lying on a stochastic attractor, and determining the conditions under which $F(\omega)$ attains a maximum. As follows from the detailed computations in Ref. [31], the effect of increasing the amplitude of the spectral peak of $F(\Omega)$ in the SR regime is reliably detected both in the absence and in the presence of noise, and is independent of the chosen magnitude of ε in the range $10^{-4} \leqslant \varepsilon \leqslant 10^{-1}$ and of the selected initial domain $x \pm \varepsilon/2$ on the attractor.

We note that the above method of analyzing the spectrum $F(\omega)$ of the recurrence time probability density $p(\tau_r)$ allows diagnosing the effect of SR on a qualitative level, but does not provide its quantitative details (the signal-to-noise ratio and the amplification coefficient), which should be computed using the appropriate realizations x_n in system (21).

6. Recurrence time characteristics and the attractor dimension in the local approach

The link between the dimension of chaotic sets in the phase space of a dynamical system and the probability that the trajectory visits the ε-vicinity of a given set point $x_0 \pm \varepsilon/2$ is defined by relations (2) and (3). By virtue of the Kac theorem in form (3), the dimension d_f is related to the mean Poincaré recurrence time. We discuss this in more detail.

For homogeneous chaotic sets endowed with a continuous and smoothly varying probability measure, finding the dependence of mean recurrence times on ε in accordance with Eqns (1) and (2) is not difficult. An illustration can be provided by the result presented in Fig. 3 for the one-dimensional map (11), from which it follows that $d_f = N = 1$, where N is the dimension of the phase space of one-dimensional system (11). This result is a consequence of the fact that the distribution $p(x)$ is a sufficiently smooth function on the attractor of system (11) (see Fig. 1).

Generally, attractors of chaotic systems have complex fractal structures, and therefore the equality $d_f = N$ does not hold. We offer an explanation and confirm it with pertinent computations.

We write the expression for the probability in Eqn (2) as

$$P(\mathbf{x}_0, \varepsilon) = \int_{x_0^1-\varepsilon/2}^{x_0^1+\varepsilon/2} \ldots \int_{x_0^N-\varepsilon/2}^{x_0^N+\varepsilon/2} p(x^1, \ldots, x^N)\, \mathrm{d}x^1 \ldots \mathrm{d}x^N, \tag{23}$$

where $p(x^1, \ldots, x^N)$ is the N-dimensional probability density on the attractor and N is the dimension of the system phase space. Without loss of generality, we limit ourselves to systems with the dimension $N = 2$, which we explore in what follows. In the case $N = 2$, we set $x^1 \equiv x$ and $x^2 \equiv y$ and rewrite Eqn (23) as

$$P(x_0, y_0, \varepsilon) = \int_{x_0-\varepsilon/2}^{x_0+\varepsilon/2} \int_{y_0-\varepsilon/2}^{y_0+\varepsilon/2} p(x, y)\, \mathrm{d}x\, \mathrm{d}y, \tag{24}$$

where (x_0, y_0) is a selected point of the attractor, placed at the center of a square of side $\varepsilon \ll 1$.

If the density $p(x, y)$ is a sufficiently smooth function of coordinates defined in the entire ε-vicinity of the selected point (x_0, y_0), by virtue of the mean value theorem (taking the smallness of ε into account), we have

$$P(x_0, y_0, \varepsilon) \simeq p(x_0, y_0) \int_{x_0-\varepsilon/2}^{x_0+\varepsilon/2} \int_{y_0-\varepsilon/2}^{y_0+\varepsilon/2} \mathrm{d}x\, \mathrm{d}y = p(x_0, y_0)\varepsilon^2. \tag{25}$$

From Eqns (1) and (25), it then follows that

$$\langle \tau(\varepsilon) \rangle = \frac{1}{p_0(x_0, y_0)}\, \varepsilon^{-2} = K\varepsilon^{-2}, \tag{26}$$

or

$$\ln \langle \tau(\varepsilon) \rangle = C - 2 \ln \varepsilon, \tag{27}$$

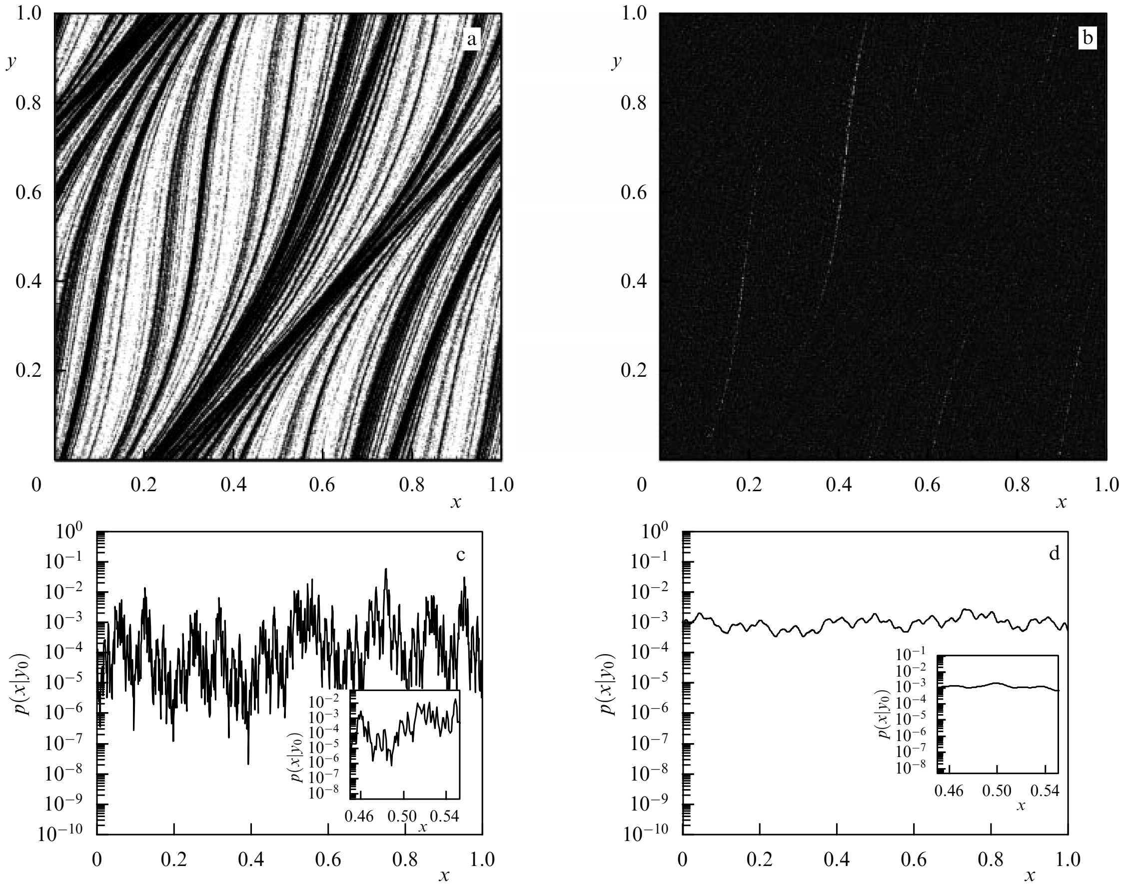

Figure 12. The attractor of system (30) obtained for the number of iteration (a) 10^6 and (b) 10^8 and the one-dimensional probability density $p(x)$ for $y = 0.5$ (c) in the absence of noise and (d) in the presence of additive noise of the intensity $D = 10^{-5}$. The results are obtained for $\delta = 0.15$. The insets in panels c and d present the distribution $p(x|y_0)$ in the ε-interval $0.45 \leqslant x \leqslant 0.55$, $y_0 = 0.5$.

where $C = \ln K = -\ln p(x_0, y_0)$, after taking the logarithm of Eqn (26). Dependence (27) is a straight line with the slope $k = 2$ and intercept C.

If $p(x, y)$ is a fractal function, relation (25) is no longer valid, and expression (27) has to be taken in a more general form (2):

$$P(x_0, y_0, \varepsilon) = p(x_0, y_0)\, \varepsilon^{-d_f}, \qquad d_f \leqslant 2, \tag{28}$$

where d_f is the fractal dimension of the set. We note that expression (28) becomes more accurate as ε decreases. With Eqn (28), we obtain

$$\ln \langle \tau(\varepsilon) \rangle = C - d_f \ln \varepsilon, \qquad d_f \leqslant 2. \tag{29}$$

Computing $\ln \langle \tau(\varepsilon) \rangle$ for different values of ε and approximating the results by straight line (29), it is possible to find the values of d_f and C.

We present the results of numerical computations obtained with the help of Eqn (29) using the modified Arnold's map [43] as an example:

$$\begin{aligned} x_{n+1} &= x_n + y_n + \delta \cos 2\pi y_n \pmod 1, \\ y_{n+1} &= x_n + 2y_n \pmod 1, \end{aligned} \tag{30}$$

where (mod 1) means taking the fractional part of the result. Map (30), which is a bijection of a unit square on the (x, y) plane into itself, belongs to the class of hyperbolic maps. For $\delta < 1/(2\pi)$, map (30) is dissipative and has a chaotic attractor with a positive largest Lyapunov exponent $\lambda_1 > 0$. The distinct feature of map (30) is that despite the contraction of phase volume, the phase trajectory visits any element of the unit square, covering it everywhere dense as $n \to \infty$. As a result, the metric dimension of the attractor of system (30) (its Kolmogorov capacity) equals an integer number ($D_C = 2$); hence the name 'chaotic ($\lambda_1 > 0$) nonstrange ($D_C = 2$) attractor'. The everywhere dense covering of the unit square by trajectories as $t \to \infty$ ensures that the probability measure $\mu(x, y)$ on the attractor is defined for any point of the square.

We consider the results of numerical experiment [44]. Figure 12 illustrates the attractor formation in system (30). For a small number of iterations (Fig. 12a), generally speaking, a nonuniform attractor forms. As the number of iterations increases, the points of the attractor cover the unit square everywhere dense (Fig. 12b). The probability density (Fig. 12c) is defined on the whole set of points (x, y) belonging to the unit square, but has a rather intricate structure, which reflects the nonuniformity of the point distribution on the attractor. This structure is most probably a fractal one, as is evidenced by the inset in Fig. 12c, showing the conditional distribution $p(x|y_0)$ for x in the ε-vicinity $0.45 \leqslant x \leqslant 0.55$. The distribution $p(x)$ in the ε-interval demonstrates a high degree of inhomogeneity, as does the distribution $p(x)$ on the unit interval. It is due to the complex character of the distribution $p(x, y)$ on the attractor of system (30) that although the Kolmogorov capacity of this attractor is $D_C = 2$, its information dimension D_I is always less than D_C and depends on the parameter δ.

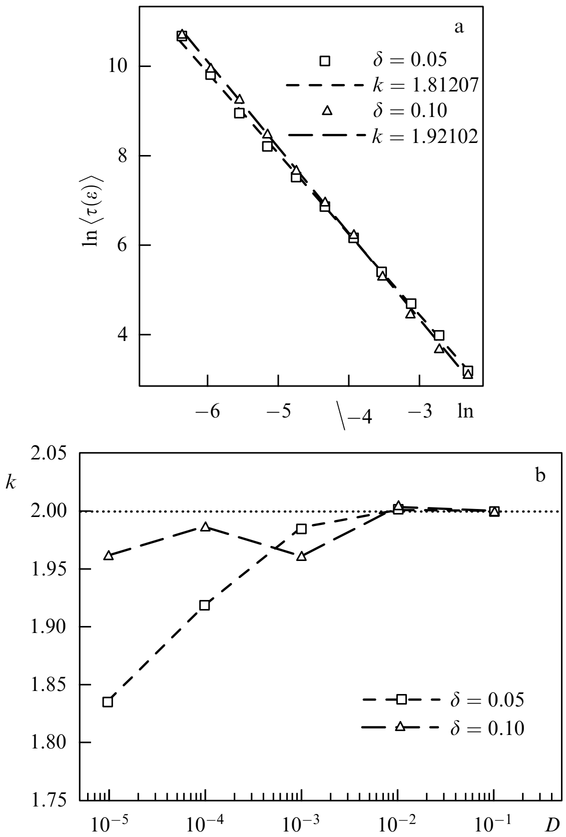

Figure 13. (a) The ε dependence of the mean time of the Poincaré recurrence for the ε-vicinity of the point $x_0 = y_0 = 0.5$ for map (30) in the absence of noise. (b) The dependence of the slope of the lines in panel (a) on the noise intensity for $\delta = 0.05$ and 0.10.

Because the density $p(x, y)$ is a fractal function, we can expect the dependence $\ln \langle \tau_{\mathrm{r}}(\varepsilon) \rangle$ for system (30) to correspond to expression (29) with a slope $d_{\mathrm{f}} < 2$. On introducing additive noise into the first equation in (30), the density $p(x, y)$ is smoothed out and the fractality disappears (see the inset in Fig. 12d). In this case, relation (27) is valid and the slope of straight line (29) should be close to 2. This is confirmed by the results of numerical experiment [44]. We used the following algorithm. An initial point with coordinates $x_n = x_0$, $y_n = y_0$ was selected at the center of a square with edge ε. Map (30) was then iterated, and the sequence of discrete time instants n_k $(k = 1, 2, \ldots, k_{\max})$, which correspond to visits to the ε-vicinity, was recorded. Given n_k, the sequence of recurrence times $\tau_k = n_{k+1} - n_k$ was computed together with mean value (3),

$$\langle \tau(\varepsilon) \rangle = \frac{1}{k_{\max}} \sum_{k=1}^{k_{\max}} (n_{k+1} - n_k) \,. \tag{31}$$

Computations have been carried out for $\delta = 0.05$, 0.10, $x_0 = 0.5$, $y_0 = 0.5$, and $k_{\max} = 10^7$. In Fig. 13a, the squares and triangles show the results of computations of $\ln \langle \tau(\varepsilon) \rangle$ for $\delta = 0.05$ and 0.10, and the dashed lines give approximations of the respective dependences. For the coefficients d_{f}, we found the values 1.81 (for $\delta = 0.05$) and 1.92 (for $\delta = 0.10$), which are certainly smaller than 2. To verify the results obtained (Fig. 13a), we computed the dependence of the slope coefficients d_{f} on the intensity of external noise, presented in Fig. 13b. For the noise intensity $D \geqslant 0.01$, the coefficient d_{f} attains the value $d_{\mathrm{f}} = 2 = N$ both for $\delta = 0.05$ and for $\delta = 0.10$. Adding noise to system (30) leads to a smoothed density $p(x, y)$, while fractality disappears and the description offered by Eqn (27) becomes applicable.

As follows from the results in Fig. 13a, the slope of the approximating lines is $d_{\mathrm{f}} < 2$. This implies that the fractal dimension d_{f} of the attractor, given by Eqns (28) and (29), should serve as a theoretical estimate for the slope coefficient. The question is how to estimate this dimension. The capacity $D_{\mathrm{C}} = 2$ cannot be used to estimate d_{f} for the attractor of system (30). It was conjectured in [23] that d_{f} can be estimated by the information dimension

$$D_{\mathrm{I}} = \lim_{\varepsilon \to 0} \frac{I(\varepsilon)}{\ln (1/\varepsilon)} \,, \quad I(\varepsilon) = -\sum_{i=1}^{M(\varepsilon)} P_i \ln P_i \,, \tag{32}$$

where $I(\varepsilon)$ is the entropy, $P_i = P(\varepsilon_i)$ is the probability that the trajectory visits the domain ε_i, and $M(\varepsilon)$ is the number of squares with the side ε covering the attractor.

The proposal in Ref. [23], however, has not been supported by numerical computations and must be tested. As follows from the data presented in Fig. 13a, $d_{\mathrm{f}} = 1.81$ for $\delta = 0.05$ and $d_{\mathrm{f}} = 1.92$ for $\delta = 0.10$. Informational dimension (32) for the attractors of system (30) is $D_{\mathrm{I}} = 1.96$ for $\delta = 0.05$ and $D_{\mathrm{I}} = 1.84$ for $\delta = 0.10$. The results of computations can be interpreted to favor the estimate for d_{f} as the information dimension D_{I}, but this assertion requires detailed numerical studies of other systems.

7. Dimension of the Afraimovich–Pesin recurrence time sequence. Global analysis

As discussed in Section 2, the minimum recurrence time (6) obtained by averaging over the entire set obeys theoretical laws (7), (9), and (10). For sets with zero topological entropy, $h_{\mathrm{t}} = 0$, Eqn (9) is valid, but if $h_{\mathrm{t}} > 0$, then Eqn (10) must be used. It has been found that if the system dynamics are characterized by at least one positive Lyapunov exponent, then $h_{\mathrm{t}} > 0$. In the absence of positive exponents in the spectrum of Lyapunov characteristic exponents, $h_{\mathrm{t}} = 0$.

To compute the dependences $\langle \tau_{\inf}(\varepsilon) \rangle$, we use the algorithms and related software described in Refs [4, 28]. The software has been tested using the example of the logistic map $x_{n+1} = \alpha x_n (1 - x_n)$ at its critical point $\alpha_{\mathrm{cr}} \approx 3.57$ and in the chaos domain $(\alpha > \alpha_{\mathrm{cr}})$. Computations confirmed the correspondence between the numerical experiment and theory: Eqn (9) holds for $\alpha = \alpha_{\mathrm{cr}}$ and Eqn (10) holds for $\alpha > \alpha_{\mathrm{cr}}$. We note that the algorithm for computing $\langle \tau_{\inf} \rangle$ was implemented in two ways [44]. The first is as follows: the attractor is covered by a union of squares of side ε, whose number depends on the value of ε. We select m points in each ε-cell. The map is then iterated from each point until the first return to the initial cell. The minimum recurrence time is determined from the data as the mean over the ensemble of initial points. The second way also starts by covering the attractor with a set of cells of size ε. A single point is selected inside each cell. The map is then repeatedly integrated to obtain a sequence of return times for each cell, and $\tau_{\inf}^{i}$ is defined from these sequences of return times for each i-cell, and then the mean minimum recurrence time is obtained by averaging over the set of cells. Because of the ergodicity of chaotic systems, the first and the second approach should lead to identical results.

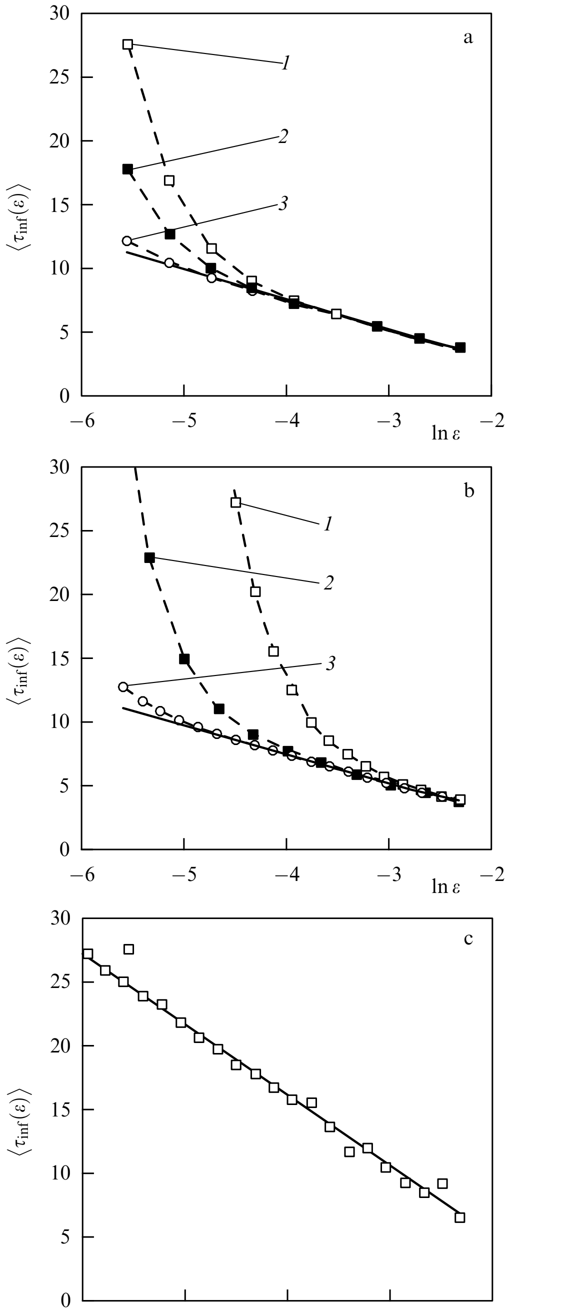

Figure 14. The dependences of the minimum mean recurrence time on the size ε: (a) for system (30), obtained for different numbers m of initial points in cells (*1*, $m = 10^4$; *2*, $m = 2.25 \times 10^4$; *3*, $m = 9 \times 10^4$), $k = 2.367$, $\alpha_c = 0.845$; (b) for system (30), obtained for different numbers m of returns into each ε-cell (*1*, $m = 10^3$; *2*, $m = 10^4$; *3*, $m = 10^5$), $k = 2.283$, $\alpha_c = 0.876$; (c) for system (33).

As an example of numerical computation of the AP dimension, we consider results pertaining to two-dimensional Arnold's map (30), which is a hyperbolic system. Relations (7), (9), and (10) have been proved precisely for such systems.

Computations indicate that in the domain $0 < \delta \leqslant 0.16$, the largest Lyapunov exponent of the attractor of system (30) is positive and depends sufficiently smoothly (without troughs reaching zero) on the parameter by virtue of hyperbolicity [44]. This points to the positivity of topological entropy and serves as a rationale to expect law (10) to be observed.

The results of computations performed in both ways are presented in Fig. 14. For a sufficiently large number of initial points in a cell ($m \approx 10^5$) (Fig. 14a) and a sufficiently large number of returns ($m \approx 10^5$) (Fig. 14b), the dependences $\langle \tau_{\rm inf}(\varepsilon) \rangle$ in the interval $-5 \leqslant \ln \varepsilon \leqslant -2$ are practically approximated by straight lines, lending support to relation (10). The slopes of the lines ($k = 2.36$ and $k = 2.28$) and the respective values of the AP dimensions, $\alpha_c = 0.84$ and $\alpha_c = 0.87$, turn out to be close. If the number of initial points in the cell is insufficiently large (Fig. 14a) or the number of returns to the cell ε is small (Fig. 14b), the dependences $\langle \tau_{\rm inf}(\varepsilon) \rangle$ do not fit to a line, but represent exponentially decreasing functions. Curiously, if these exponential dependences are used and results are viewed in coordinates $(\ln \langle \tau_{\rm inf}(\varepsilon) \rangle, \ln \varepsilon)$, we obtain straight lines that correspond to Eqn (9). These results are erroneous, however, and are related to the insufficient number of initial points or returns into a cell.

Because of the fractality of the density distribution $p(x, y)$ on the attractor of system (30), computing the characteristics of the Poincaré recurrence times requires particular care and substantial computational time in both local and global approaches. These difficulties can be greatly reduced if we choose the two-dimensional map as the Lozi map [45]

$$
\begin{aligned}
x_{n+1} &= 1 - \alpha |x_n| + y_n \,, \quad & 1.3 \leqslant \alpha \leqslant 1.8 \,, \\
y_{n+1} &= \beta x_n \,, & \beta = 0.3 \,.
\end{aligned}
\tag{33}
$$

It is well known that the Lozi map is characterized by a quasihyperbolic chaotic attractor [32] and suits the test experiments in the best way, because it has ergodic properties assumed in theoretical proofs of relations (9) and (10). The results of computations performed for a chaotic attractor in system (33) are presented in Fig. 14c. As can be seen from the figure, the dependence $\langle \tau_{\rm inf}(\varepsilon) \rangle$ on $\ln \varepsilon$ is well approximated by a straight line with the slope $k = 5.551$, which perfectly agrees with expression (10). For the AP dimension, we find $\alpha_c = d/k \approx 0.19$, where $d = 1.05$ (the dimension of the Lozi attractor).

8. Correspondence between the Afraimovich–Pesin dimension, the Lyapunov exponents, and the entropy of the system

The AP dimension characterizes the degree of complexity of the Poincaré recurrence time sequence [37]. But the connection of the AP dimension with the dynamical and geometrical characteristics of the attractor in the system [46] requires a deeper analysis.

A fundamental result in this area is the proof of the conjecture that for one-dimensional maps with chaotic dynamics, the AP dimension coincides numerically with the positive Lyapunov exponent [47]. We illustrate this result numerically with the example of the logistic map

$$
x_{n+1} = r x_n (1 - x_n) \,, \tag{34}
$$

where x is the dynamical variable and r is the control parameter. In logistic map (34), the transition to chaos is realized via a sequence of period doubling bifurcations. The transition to chaos is illustrated with the help of the

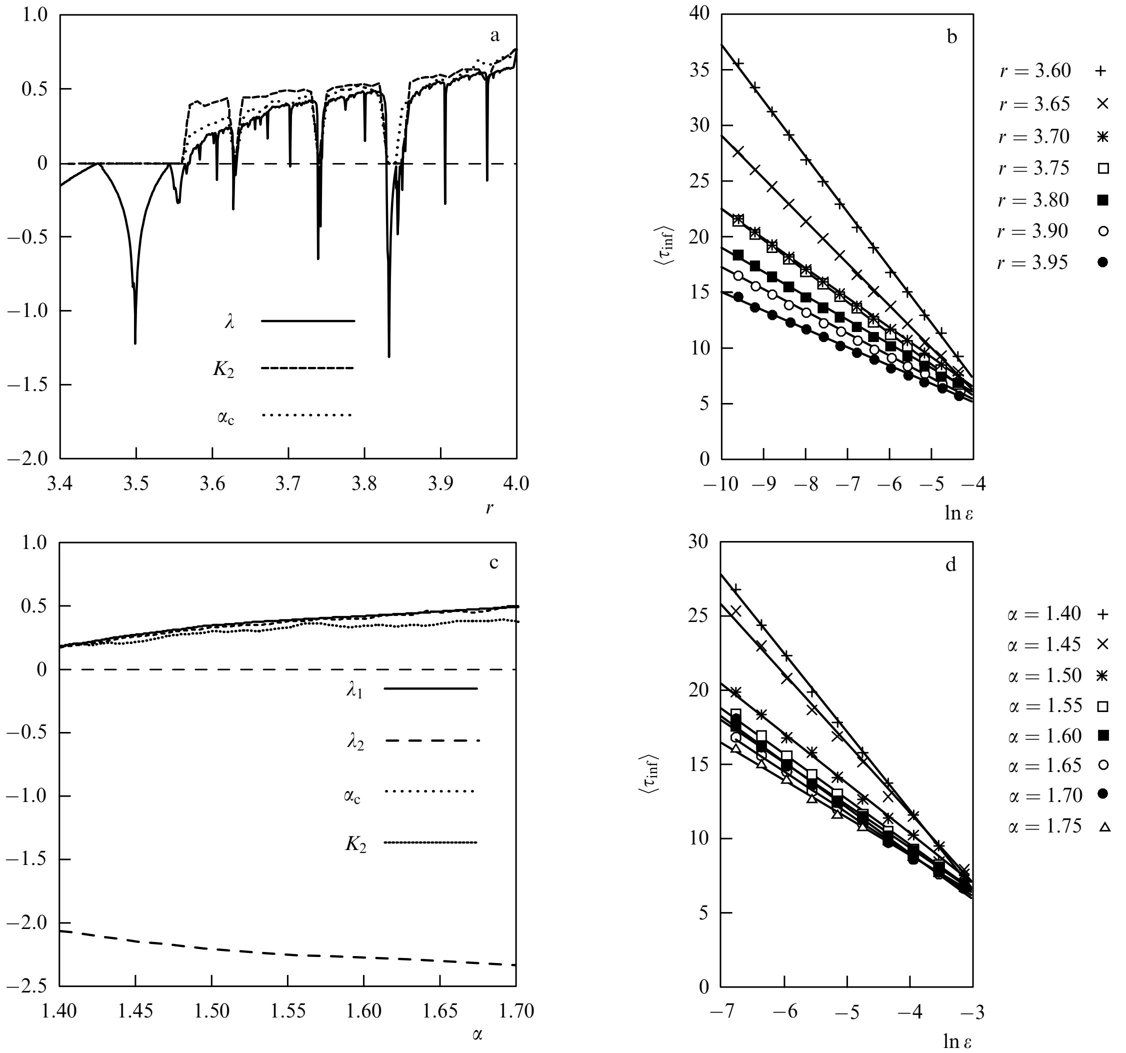

Figure 15. (a) The characteristic Lyapunov exponent λ, the KS entropy K_2, and the AP dimension α_c of logistic map (34) as functions of the control parameter r. (b) The minimum mean Poincaré recurrence time (6) as a function of $\ln\varepsilon$ in system (34) for various values of the control parameter r. (c) The spectrum of characteristic Lyapunov exponents $\lambda_{1,2}$, the KS entropy K_2, and the AP dimension α_c of Lozi map (33) as functions of the control parameter α for $\beta = 0.3$. (d) The minimum mean Poincaré recurrence time (6) as a function of $\ln\varepsilon$ in system (33) for different values of the control parameter α for $\beta = 0.3$.

dependence of the characteristic Lyapunov exponent on the parameter r (Fig. 15a).

In what follows, we use the control parameter values $r \in [3.57, 4.00]$ corresponding to the regime of deterministic chaos in the system. As can be seen from Fig. 15b, the mean minimum Poincaré recurrence time for logistic map (34) in the regime of deterministic chaos for the global approach, Eqn (6), depends not only on the cell size ε but also on the value of the control parameter r. We note that the plots in Fig. 15b are straight lines in a logarithmic scale. This corresponds to theoretical results in Ref. [16], which are based on the assumption that $\langle\tau_{\inf}(\varepsilon)\rangle$ obeys law (10) when the dynamical system has a positive topological entropy (see Section 7 and Fig. 14). The value of α_c can be found from the slope k of the lines in Fig. 15b if the dimension d of the attractor in system (34) is known:

$$k = -\frac{d}{\alpha_c}\,. \tag{35}$$

For $r = 4$, map (34) has a smooth probability density $p(x)$ that can be determined analytically [48, 49]. The results of computations indicate that in the interval $r \in [3.57, 4.00]$, excluding the periodicity windows, the distribution $p(x)$ remains piecewise constant. It this case, as discussed in Section 6, relation (23) holds, where we must set $N = 1$ (one-dimensional map) and take the attractor dimension $d = 1$, which coincides with the dimension of system (34). It then follows from Eqn (35) that $\alpha_c = -1/k$.

It is shown in [47, 50] for map (34) that α_c coincides with the value of the characteristic Lyapunov exponent and the KS entropy, which is apparent from Fig. 15a.

The results in Refs [47, 50] and our computations (Fig. 15b) confirm the rigorous mathematical conclusion in Ref. [47], derived in application to one-dimensional maps. A question arises: Can we assume that the correspondence established between the Lyapunov exponent and the AP dimension of the Poincaré recurrences extends to two-dimensional systems [51]? The following argument may serve as the rationale. It is well known that three-dimensional differential systems with chaotic attractors are characterized by two-dimensional Poincaré maps in their cross sections. If the dissipation is sufficiently high, a two-dimensional map can be approximately replaced by a one-dimensional map [52]. On this basis, it can be proposed that the theorem in Ref. [47] can be applied to two-dimensional maps that have a single positive exponent in the regime of chaos. We test this statement. We consider Lozi map (33), which is one of the simplest examples of two-dimensional chaotic systems. From Fig. 15c, which shows the spectrum of characteristic Lyapunov exponents for $\beta = 0.3$, we see that in the control parameter range $\alpha \in [1.32, 1.75]$, system (33) demonstrates chaotic dynamics on its quasihyperbolic attractor, with the dimension $d \approx 1.1$.

We consider the Poincaré recurrence time for the chaotic attractor of the Lozi map from the standpoint of the global approach. The quantity $\langle \tau_{\inf}(\varepsilon) \rangle$, displayed in Fig. 15d as a function of the covering cell size ε for various values of the control parameter α, does not differ qualitatively from that obtained for logistic map (34). From Fig. 15c, which presents the KS entropy, the AP dimension, and the spectrum of characteristic Lyapunov exponents as functions of the control parameter, it can be readily deduced that λ_1, K_2, and α_c practically coincide [51].

The fact that the value of α_c practically coincides with the largest Lyapunov exponent ($\alpha_c \approx \lambda_1$) for one- and two-dimensional maps with chaotic attractors can be used to estimate the fractal dimension of the map given by Eqn (35). Determining the slope k when computing $\langle \tau_{\inf}(\varepsilon) \rangle$ from relation (10), we can find the fractal dimension $d = \lambda_1 |k|$. We note that we obtain the fractal dimension of the attractor as a whole, and not the local dimension, as in the situation described in Section 6.

In the theoretical analysis in the framework of the global approach (see, e.g., Ref. [4]), it is implied that the Hausdorff dimension of a set or its estimate as the Kolmogorov capacity is taken in (10). Accordingly, determining the slope k from the plots of $\langle \tau_{\inf}(\varepsilon) \rangle$, it is possible to determine the Hausdorff dimension d_f. Other estimates of the dimension are also known (capacity, information dimension, correlation, and Lyapunov dimension [43]). Based on our experience of computing d_f and comparing the results with the computed capacity and information dimension with the use of classical definitions and algorithms, we can speculate that all estimates of dimension are close to d_f given by (10). However, there are currently no grounds to argue that we have a clear answer to the question of which dimension is closer to the Hausdorff dimension d_f. For instance, for logistic map (34), d_f practically coincides with the capacity dimension, but for modified Arnold's map (39), the estimate of d_f is given by the information dimension. It is worthwhile to continue research in this area.

From the physical standpoint, an interesting perspective is to explore the influence of white Gaussian noise on the relations established among the AP dimension, characteristic Lyapunov exponents, and the KS entropy. We mention that for a system with noise, we use the *relative metric entropy* [53, 54] instead of the KS entropy.

We start from the case of a one-dimensional map. We rewrite Feigenbaum map (34), by adding the source of white Gaussian noise ξ of intensity D:

$$x_{n+1} = r x_n (1 - x_n) + \sqrt{2D}\, \xi_n \,. \tag{36}$$

Under the action of noise, the correspondence between the relative metric entropy and characteristic Lyapunov exponents is violated [53]. We fix the control parameter $r = 3.7$ and, increasing D, follow the change in the characteristic Lyapunov exponent and relative metric entropy of the system.

As can be seen from Fig. 16a, as the noise intensity D increases, the AP dimension also increases, maintaining good agreement with the relative metric entropy $\hat{K}_2$. This correspondence is also preserved under variations of the control parameter. At the same time, Fig. 16a shows that the Lyapunov exponent is practically insensitive to the noise intensity.

The results presented in Figs 16a and 17a, b invite the assumption that for noisy one-dimensional chaotic maps, the AP dimension α_c is not related to the characteristic Lyapunov exponent, but its value is close to that of the entropy $\hat{K}_2$. We check in what follows whether this correspondence is valid for a two-dimensional map.

We add a source of the Gaussian white noise ξ of intensity D to Lozi map (33):

$$\begin{aligned} x_{n+1} &= 1 - \alpha |x_n| + y_n + \sqrt{2D}\, \xi_n \,, \\ y_{n+1} &= \beta x_n \,. \end{aligned} \tag{37}$$

The dependence of the largest characteristic Lyapunov exponent, the relative metric entropy, and the AP dimension on the value of the control parameter is presented in Fig. 17c, d for several values of the noise intensity. The connection between the relative metric entropy and largest Lyapunov exponent disappears as the noise intensity increases. Yet the correspondence between the AP dimension and the largest characteristic Lyapunov exponent is preserved. Having fixed the control parameters $\alpha = 1.4$ and $\beta = 0.3$, we compute α_c and $\hat{K}_2$ as functions of the noise intensity. As can be seen from Fig. 16b, which displays the results of these computations, the quantitative correspondence between α_c and $\hat{K}_2$ persists as the noise intensity is varied.

We test the validity of our assumptions using two more examples of chaotic two-dimensional maps in the presence of noise. The first is the Hénon map, which falls into the class of nonhyperbolic systems [55],

$$\begin{aligned} x_{n+1} &= 1 - \alpha x_n^2 + y_n + \sqrt{2D}\, \xi_n \,, \\ y_{n+1} &= \beta x_n \,, \end{aligned} \tag{38}$$

where x and y are the phase variables, α and β are the control parameters, and ξ is the source of white noise of intensity D.

System (38) demonstrates the regime of chaotic quasi-attractors in the absence of noise for $\alpha = 1.4$ and $\beta = 0.3$. In this case, the quasi-attractor has the dimension $b \approx 1.25$. We fix the values of control parameters and compute the largest characteristic Lyapunov exponent, the relative metric entropy, and the AP dimension by varying the noise intensity. From Fig. 16c, it can be inferred that the correspondence between the AP dimension and relative metric entropy, found for Lozi map (33), is also valid for the Hénon map. This result is of interest because the Lozi map is an example of a quasi-hyperbolic system, while the Hénon map is a nonhyperbolic system.

Finally, we consider hyperbolic modified Arnold's map (30) with an additive source of white Gaussian noise ξ of

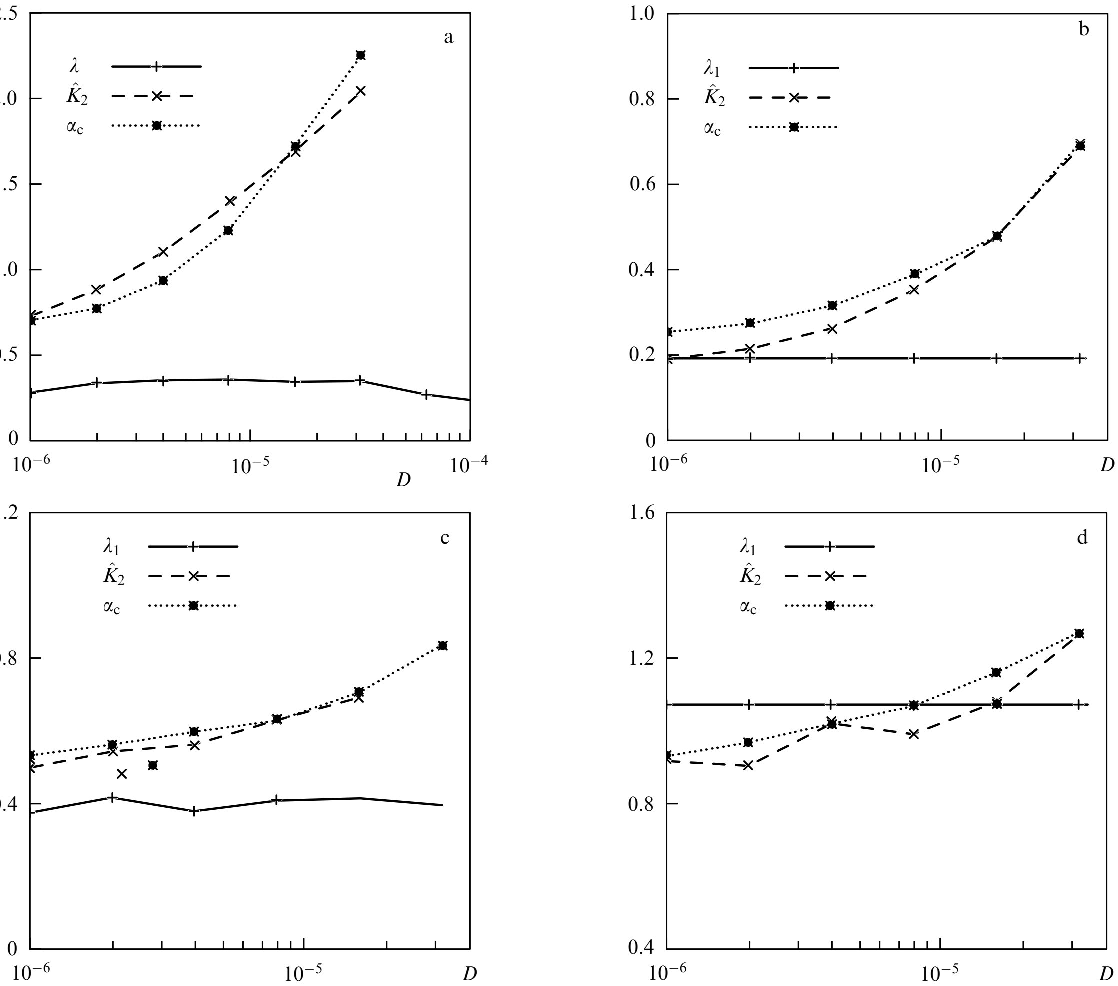

Figure 16. The largest characteristic Lyapunov exponent λ_1, the relative metric entropy $\hat{K}_2$, and the AP dimension α_c in the presence of noise for (a) logistic map (36) for $r = 3.7$, (b) Lozi map (37) for $\alpha = 1.4$ and $\beta = 0.3$, (c) Hénon map (38) for $\alpha = 1.4$ and $\beta = 0.3$ and (d) modified Arnold's map (30) for $\delta = 0.1$.

intensity D:

$$x_{n+1} = x_n + y_n + \delta\cos(2\pi y_n) + \sqrt{2D}\,\xi_n \pmod 1\,, \qquad y_{n+1} = x_n + 2y_n \pmod 1\,. \tag{39}$$

The dependences of λ_1, $\hat{K}_2$, and α_c on the noise intensity D are plotted in Fig. 16d. As in the two preceding cases, our conclusion on the correspondence between the relative metric entropy and the AP dimension remains valid [51].

The results presented above on the correspondence between the AP dimension of systems affected by noise and the relative metric entropy $\hat{K}_2$ are currently a purely experimental fact. The cause of such a correspondence is quite possibly that both the AP dimension and the entropy $\hat{K}_2$ are introduced based on the Poincaré recurrence concept. These results will hopefully be given a rigorous mathematical proof in the future.

9. Diagnostics of the effect of synchronization for stochastic self-oscillations with the help of the Afraimovich–Pesin dimension

The AP dimension is a global characteristic of a sequence of recurrence times pertaining to the system attractor as a whole and can be used as a criterion of synchronization of chaotic self-oscillations. For example, we consider the effect of chaos synchronization in two coupled Lorentz oscillators, described in Ref. [28]. The equations for this system have the form

$$\begin{aligned}
\dot{x}_1 &= \sigma_1(x_2 - x_1) + c_1(y_1 - x_1)\,,\\
\dot{x}_2 &= \rho_1 x_1 - x_2 - x_1x_3 + c_2(y_2 - x_2)\,,\\
\dot{x}_3 &= -\beta_1 x_3 + x_1x_2 + x_3(y_3 - x_3)\,,\\
\dot{y}_1 &= \sigma_2(y_2 - y_1) + c_1(x_1 - y_1)\,,\\
\dot{y}_2 &= \rho_2 y_1 - y_2 - y_1y_3 + c_2(x_2 - y_2)\,,\\
\dot{y}_3 &= -\beta_2 y_3 + y_1y_2 + y_3(x_3 - y_3)\,.
\end{aligned} \tag{40}$$

The phase variables x_i and y_i, $i = 1, 2, 3$ are respectively related to the first and second Lorentz systems. Slightly detuned oscillators are considered for the following values of control parameters:

$$\rho_1 = \rho_2 = 45.92\,, \quad \sigma_1 = 16.0, \quad \sigma_2 = 16.02\,, \qquad \beta_1 = 4.0\,, \quad \beta_2 = 4.01\,.$$

The effect of synchronization can be achieved by increasing the coupling between the oscillators, which depends on the coefficients c_1, c_2, and c_3 in Eqns (40).

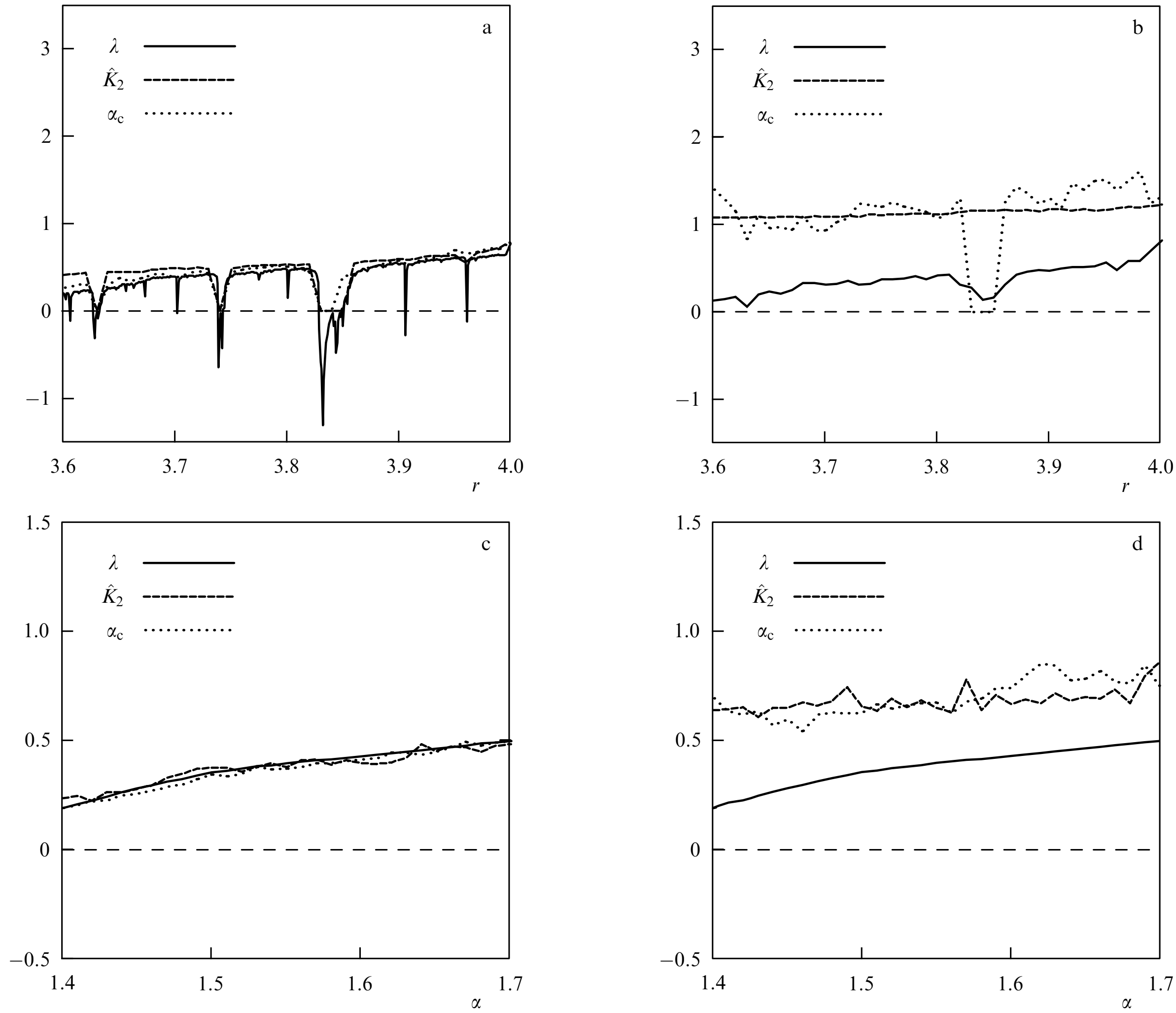

Figure 17. The characteristic Lyapunov exponent λ, the relative metric entropy $\hat{K}_2$, and the AP dimension α_c for (a) logistic map (36) with $D = 0$, (b) the same as in (a) but in the presence of noise with $D = 4 \times 10^{-4}$, (c) Lozi map (37) with $\beta = 0.3$ and the noise intensity $D = 10^{-6}$, and (d) the same as in (c) but with the noise intensity $D = 3.2 \times 10^{-5}$.

In the absence of coupling ($c_i = 0$), the chaotic attractor of system (40) is located in a six-dimensional phase space because of the detuning in the parameters σ and β. Figure 18a shows the projection of the chaotic attractor on the plane of phase variables (x_1, y_1). Projections on the planes (x_2, y_2) and (x_3, y_3) are qualitatively similar.

If the coupling is strengthened, the effect of topological chaos synchronization is realized [28]. In this case, the attractor of system (40) is located in the vicinity of the invariant three-dimensional subspace $\mathbf{x} \approx \mathbf{y}$ $(x_1 \approx y_1, x_2 \approx y_2, x_3 \approx y_3)$. The projections of a phase trajectory on the planes (x_i, y_i) should be confined to a close vicinity of the diagonal $x_i = y_i$ $(i = 1, 2, 3)$. Computations confirm the anticipated result, which is demonstrated in Fig. 18b. Because of the small detuning of the Lorentz oscillators with respect to the parameters, a regime of practically complete synchronization is realized in system (40) experimentally upon introducing the coupling, which is only possible if the coupled systems are identical [56]. Strictly speaking, we are dealing with topological synchronization in the example considered, in which there are differences between the variables x_i and y_i $(i = 1, 2, 3)$. Computations indicate that the quantity $|x_i(t) - y_i(t)|$, albeit small if averaged over time, remains finite, of the order of 10^{-4}. It cannot be discerned in Fig. 18b.

We discuss the results of computations of the AP dimension for the attractors of subsystems (40) in the absence of coupling and in the synchronization regime.

As follows from Fig. 18c, d, the computed dependences of $\langle \tau_{\mathrm{inf}}(\varepsilon) \rangle$ obey theoretical law (10), because we are dealing with chaotic regimes with a positive topological entropy. The slopes of the curves in Fig. 18c, $k = d/\alpha_c$, are different because of the detuning in the parameters and the absence of coupling. In this case, the values of α_c are naturally different: for the first Lorentz system, $\alpha_{c1} = d/k_1 = 0.122$, and for the second, $\alpha_{c2} = 0.110$. To compute α_{c1} and α_{c2}, we used the values of the slopes of the lines in Fig. 18, $k_1 = 16.54$ and $k_2 = 18.43$, taking the dimension of the Lorentz attractor to be $d = 2.03$.

In the synchronization regime (Fig. 18d), the dependences $\langle \tau_{\mathrm{inf}}(\varepsilon) \rangle$ for the first and second subsystems are in complete agreement. Their slopes and, consequently, AP dimensions are also equal: $k_1 = k_2 = 18.43$, $\alpha_{c1} = \alpha_{c2} = 0.11$. Thus, in the regime of full synchronization of two coupled chaotic systems, their AP dimensions equalize.

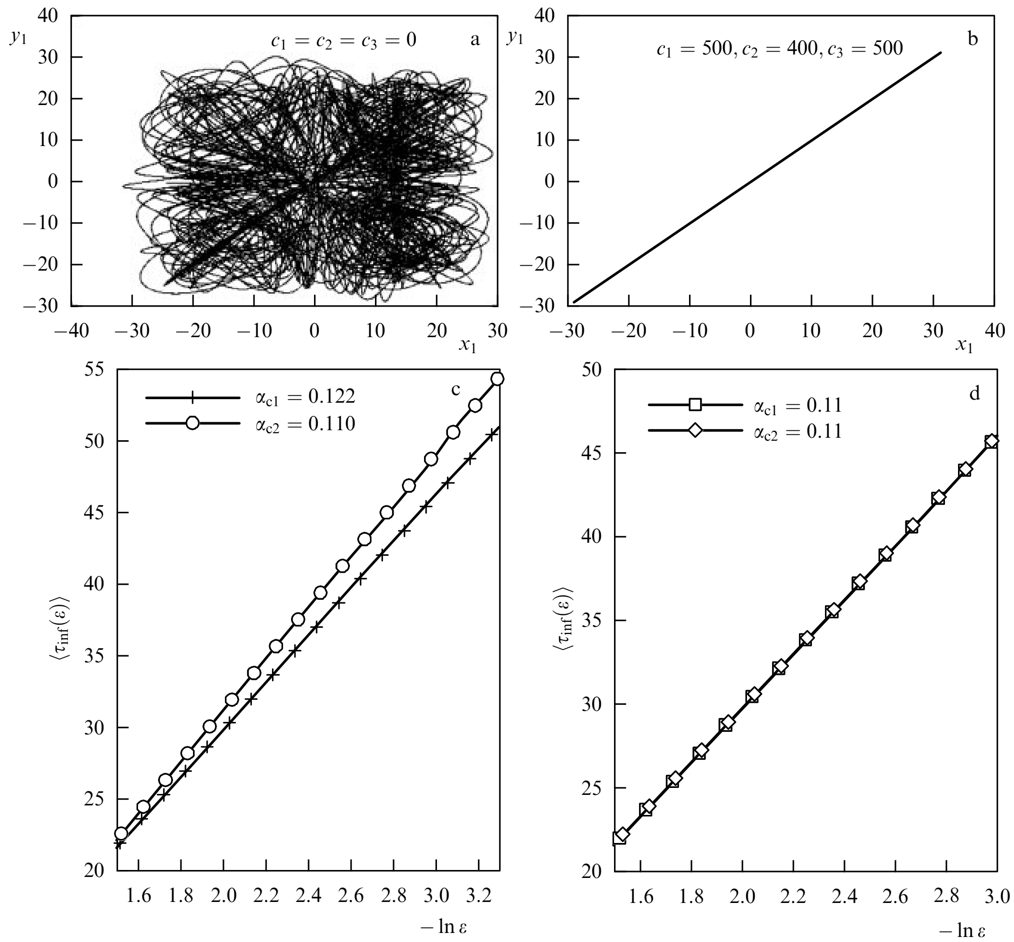

Figure 18. The projection of a six-dimensional attractor of system (40) on the plane of variables (x_1, y_1) (a) in the absence of coupling $(c_1 = c_2 = c_3 = 0)$ and (b) in the presence of coupling ($c_1 = 500$, $c_2 = c_3 = 400$). The dependences of $\langle\tau_{\inf}(\varepsilon)\rangle$ in the absence (c) and presence (d) of synchronization.

This result is rather trivial from the standpoint of the theory dealing with synchronization of stochastic oscillations and can be readily obtained by classical methods (see, e.g., Ref. [32]) with a much smaller computational effort. Its value is rather in the fact that as a statistical characteristic of a sequence of Poincaré recurrences, the AP dimension can serve as a criterion of synchronization — a fundamental phenomenon in the physics of oscillations.

10. Conclusions

The material presented in this review may serve as an introduction to a current set of questions concerning the fundamental problem of the Poincaré recurrence as applied to nonlinear dissipative systems with chaotic attractors. The review includes a discussion of the main theoretical results in the frameworks of both local and global approaches. These results are presented without resorting to rigorous mathematical proofs. Attention is focused exclusively on the results and their applicability conditions. An attempt is made to analyze the relevance of rigorous results if some deviations are allowed from the conditions assumed in the relevant theorems. We explore the influence of noise, the finiteness of the initial state neighborhood, and the lack of hyperbolicity. It is found that the rigorous results can be applied with an accuracy sufficient for physical applications for a small but finite ε-vicinity ($\varepsilon \simeq 10^{-3} - 10^{-5}$). At the same time, the finiteness of ε may lead to substantial differences between theoretical and experimental results, which can be used to diagnose the attributes of the regimes of system functioning and their characteristics. It is shown that for small ε, for example, the effect of stochastic resonance can be diagnosed.

An important result, in our opinion, is the experimental substantiation of the applicability of the Kac theorem (local approach) to the analysis of Poincaré recurrences in systems with noise. In this case, it is necessary to account for the change in the probability measure on the attractor caused by the noise perturbation.

An interesting result is also the confirmation, in numerical experiments, of the correspondence between the Afraimovich–Pesin dimension and the largest Lyapunov exponent, not only for one-dimensional (which is proved theoretically) but also for two-dimensional systems. As a result, a new method is emerging for numerically assessing the attractor dimension via computations of the Poincaré recurrence statistics in the global framework. Also important is the result on the correspondence of the AP dimension with the value of the Kolmogorov relative entropy for a system affected by noise. In this case, the correspondence between the AP dimension and the leading Lyapunov exponent is broken. From a general physical perspective, the totality of results presented in this review stems from the fact that the process of Poincaré recurrence itself reflects the system evolution with time. It is perfectly natural that the statistical characteristics of the sequence of recurrence times reflect the characteristics of the system dynamics and are related to them.

The results of solving a set of applied problems presented in this review lend support to this fact. It is proved with certainty that the statistical characteristics of the Poincaré recurrence time respond adequately to physical effects such as the stochastic resonance or synchronization, enabling one to numerically compute fractal dimensions. All this is important from the standpoint of understanding the physical aspects of the Poincaré recurrence statistics following from mathematical theory. The results discussed in the review by no means exhaust all the multitude of information hidden in the behavior of Poincaré recurrences. There is no doubt that further research in this field will serve as proof of this assertion.

It is our pleasant duty to express our deep gratitude to V S Afraimovich for the numerous fruitful discussions of the Poincaré recurrence problem and his interest in our work. We are also indebted to our colleagues and coauthors of the papers we have cited: Ya I Boev, M E Khairulin, N I Biryukova, and Yu Kurts for their help in obtaining some results presented in this review.

This work was partially supported by the Federal Program 'Scientific and Scientific-Pedagogical Personnel of Innovative Russia' (state contract 12.470.11.1182) and the Russian Foundation for Basic Research, grant 13-02-00216.

References

1. Poincaré H *Les Méthodes Nouvelles de la Mécanique Céleste* Vol. 3 (Paris: Gauthier-Villars, 1899) [Translated into English: *New Methods of Celestial Mechanics* Vol. 3 (Woodbury, NY: American Institute of Physics, 1993); translated into Russian: *Izbrannye Trudy* (Selected Works) Vol. 2 (Moscow: Nauka, 1972)]
2. Poincaré H *Acta Math.* **13** A3 (1890)
3. Nemytskii V V, Stepanov V V *Qualitative Theory of Differential Equations* (New York: Dover Publ., 1989) [Translated from Russian: *Kachestvennaya Teoriya Differentsial'nykh Uravnenii* (Moscow – Leningrad: Gostekhizdat, 1947)]
4. Afraimovich V, Ugalde E, Urías J *Fractal Dimensions for Poincaré Recurrences* (Amsterdam: Elsevier, 2006) [Translated into Russian (Moscow – Izhevsk: RKhD, 2011)]
5. Boshernitzan M D *Inventiones Math.* **113** 617 (1993)
6. Moshchevitin N G *Russ. Math. Surv.* **53** 219 (1998) [*Usp. Mat. Nauk* **53** (1) 223 (1998)]
7. Shkredov I D *Math. Notes* **72** 576 (2002) [*Mat. Zametki* **72** 625 (2002)]
8. Hirata M, Saussol B, Vaienti S *Commun. Math. Phys.* **206** 33 (1999)
9. Abadi M, Galves A *Markov Process. Relat. Fields* **7** (1) 97 (2001)
10. Haydn N, Lacroix Y, Vaienti S *Ann. Probab.* **33** 2043 (2005)
11. Kac M *Bull. Am. Math. Soc.* **53** 1002 (1947)
12. Kac M *Proc. of the Summer Seminar, Boulder, Colorado, 1957* Vol. 1 *Probability and Related Topics in Physical Sciences* (Lectures in Applied Mathematics, Vol. 1) (London: Intersci. Publ., 1959) [Translated into Russian (Moscow: Mir, 1965)]
13. Chirikov B V, Shepelyanskii D L "Statistika vozvratov Puankare i struktura stokhasticheskogo sloya nelineinogo rezonansa" ("Statistics of Poicaré recurrences and the structure of stochastic layer of a nonlinear resonance"), Preprint No. 81-69 (Novosibirsk: Inst. Yadernoi Fiziki SO AN SSSR, 1981)
14. Chetaev N *C.R. Acad. Sci. Paris* **187** 637 (1928)
15. Chetaev N G *Uchenye Zapiski Kazanskogo Univ.* (2) 198 (1929)
16. Afraimovich V *Chaos* **7** (1) 12 (1997)
17. Afraimovich V, Zaslavsky G M *Phys. Rev. E* **55** 5418 (1997)
18. Pesin Ya B *Dimension Theory in Dynamical Systems: Contemporary Views and Applications* (Chicago: Univ. of Chicago Press, 1997)
19. Penné V, Saussol B, Vaienti S *Discrete Contin. Dyn. Syst. A* **5** 783 (1999)
20. Sirvent V F *Stoch. Dyn.* **2** 599 (2002)
21. Marwan N et al. *Phys. Rep.* **438** 237 (2007)
22. Ngamga E J et al. *Phys. Rev. E* **85** 026217 (2012)
23. Gao J B *Phys. Rev. Lett.* **83** 3178 (1999)
24. Baptista M S, Kraut S, Grebogi C *Phys. Rev. Lett.* **95** 094101 (2005)
25. Altmann E G, Tél T *Phys. Rev. Lett.* **100** 174101 (2008)
26. Bolotin Yu L et al. *Nelin. Dinamika* **6** 719 (2010)
27. Adler R L, Konheim A G, McAndrew M H *Trans. Amer. Math. Soc.* **114** 309 (1965)
28. Afraimovich V S, Lin W-W, Rulkov N F *Int. J. Bifurcat. Chaos* **10** 2323 (2000)
29. Katok A, Hasselblatt B *Introduction to the Modern Theory of Dynamical Systems* (Cambridge: Cambridge Univ. Press, 1995) [Translated into Russian (Moscow: Faktorial, 1999)]
30. Afraimovich V *Taiwanese J. Math.* **3** (2) 139 (1999)
31. Anishchenko V S, Boev Y I *Commun. Nonlin. Sci. Numer. Simulat.* **18** 953 (2013)
32. Anishchenko V et al. *Nonlinear Dynamics of Chaotic and Stochastic Systems. Tutorial and Modern Development* (Berlin: Springer, 2002)
33. Benzi R, Sutera A, Vulpiani A *J. Phys. A Math. Gen.* **14** L453 (1981)
34. Kuznetsov S P *Phys. Usp.* **54** 119 (2011) [*Usp. Fiz. Nauk* **181** 121 (2011)]
35. Anishchenko V S, Khairulin M E *Tech. Phys. Lett.* **37** 561 (2011) [*Pis'ma Zh. Tekh. Fiz.* **37** (12) 35 (2011)]
36. Altmann E G, da Silva E C, Caldas I L *Chaos* **14** 975 (2004)
37. Anishchenko V S et al. *Eur. Phys. J. B* **82** 219 (2011)
38. Gammaitoni L et al. *Rev. Mod. Phys.* **70** 223 (1998)
39. Anishchenko V S et al. *Phys. Usp.* **42** 7 (1999) [*Usp. Fiz. Nauk* **169** 7 (1999)]
40. Kramers H A *Physica* **7** 284 (1940)
41. Anishchenko V S, Neiman A B, Safanova M A *J. Stat. Phys.* **70** 183 (1993)
42. Freidlin M *Physica B* **306** 10 (2001)
43. Farmer J D, Ott E, Yorke J A *Physica D* **7** (1 – 3) 153 (1983)
44. Anishchenko V S et al. *Nelin. Dinamika* **8** (1) 29 (2012)
45. Lozi R *J. Phys. Colloques* **39** C5-9 (1978)
46. Loskutov A *Phys. Usp.* **53** 1257 (2010) [*Usp. Fiz. Nauk* **180** 1305 (2010)]
47. Saussol B, Troubetzkoy S, Vaienti S *J. Stat. Phys.* **106** 623 (2002)
48. Schuster H G *Deterministic Chaos. An Introduction* (Weinheim: Physik-Verlag, 1984) [Translated into Russian (Moscow: Mir, 1988)]
49. Anishchenko V S et al. *Nelin. Dinamika* **8** 449 (2012)
50. Baptista M S, Maranhão D M, Sartorelli J C *Chaos* **19** 043115 (2009)
51. Astakhov S V, Anishchenko V S *Phys. Lett. A* **376** 3620 (2012)
52. Anishchenko V S *Slozhnye Kolebaniya v Prostykh Sistemakh* (Complex Oscillations in Simple Systems) (Moscow: Nauka, 1990)
53. Anishchenko V S, Astakhov S *Int. J. Bifurcation Chaos* **18** 2851 (2008)
54. Anishchenko V S, Astakhov S V, Vadivasova T E *Regul. Chaot. Dyn.* **15** 261 (2010)
55. Hénon M *Commun. Math. Phys.* **50** 69 (1976)
56. Pecora L M, Carroll T L *Phys. Rev. Lett.* **64** 821 (1990)